# High-resolution measurement of the $^{118,124}$Sn$(p,t)^{116,122}$Sn reactions: Shell-model and microscopic distorted-wave Born approximation calculations

P. Guazzoni and L. Zetta
*Dipartimento di Fisica dell'Università, and Istituto Nazionale di Fisica Nucleare, Via Celoria 16, I-20133 Milan, Italy*

A. Covello[1,2] and A. Gargano[2]
[1]*Dipartimento di Scienze Fisiche, Università di Napoli Federico II, Complesso Universitario di Monte S. Angelo, Via Cintia, I-80126 Naples, Italy*
[2]*Istituto Nazionale di Fisica Nucleare, Complesso Universitario di Monte S. Angelo, Via Cintia, I-80126 Naples, Italy*

B. F. Bayman
*School of Physics and Astronomy, University of Minnesota, Minneapolis, Minnesota 55455, USA*

T. Faestermann
*Physik Department TUM, D-85748 Garching, Germany*

G. Graw, R. Hertenberger, and H.-F. Wirth
*Fakultät für Physik der LMU, D-85748 Garching, Germany*

M. Jaskola
*Soltan Institute for Nuclear Studies, PL-Warsaw, Poland*
(Received 22 November 2010; published 19 April 2011)

The $^{118,124}$Sn$(p,t)^{116,122}$Sn reactions have been investigated in high-resolution experiments at incident proton energies of 24.6 and 25 MeV, respectively. Angular distributions for 55 transitions to levels of $^{116}$Sn and 63 transitions to levels of $^{122}$Sn, up to excitation energies of ∼3.850 and ∼4.000 MeV, respectively, have been measured. The spin and parity identification was carried out by means of a distorted-wave Born approximation (DWBA) analysis, performed by using conventional Woods-Saxon potentials. A shell-model study of $^{116}$Sn and $^{122}$Sn nuclei was performed using a realistic two-body effective interaction derived from the CD-Bonn nucleon-nucleon potential. The doubly magic nucleus $^{132}$Sn was assumed as a closed core, with the 16 and 10 valence neutron holes occupying the five levels of the 50-82 shell. The energy spectra have been calculated and compared with the experimental ones, and the theoretical two-nucleon spectroscopic amplitudes, evaluated in a truncated seniority space, have been used in the microscopic DWBA calculation of some cross-section angular distributions of both reactions.

DOI: 10.1103/PhysRevC.83.044614 PACS number(s): 25.40.Hs, 21.10.Hw, 21.60.Cs, 27.60.+j

## I. INTRODUCTION

Because of the existence of a large number of stable isotopes, the tin isotopes are particularly suited for studying the evolution of nuclear structure when the 50-82 neutron shell is filled.

The $(p,t)$ reaction on even Sn isotopes 112, 116, 120, and 122 [1–4] was systematically studied by our group starting from 1998. This paper, devoted to the measurement and analysis of $^{118,124}$Sn$(p,t)^{116,122}$Sn reactions, will complete the study. $^{114}$Sn has not yet been used as a target for a $(p,t)$ study because the available enrichment ($\leqslant$63%) is too low to allow a safe identification of the level energies of the residual nucleus $^{112}$Sn, because of the background presence of contributions from other, more abundant, tin isotopes.

The $(p,t)$ reactions on $^{118}$Sn and $^{124}$Sn were investigated by Fleming *et al.* [5], but only few transitions were studied. For this reason we have performed a new investigation of the $^{118,124}$Sn$(p,t)^{116,122}$Sn reactions, by means of a high-resolution experiment at the incident proton energies of 24.6 and 25 MeV, respectively. The present paper covers the excitation energy range from 0 to 3.843 MeV for $^{116}$Sn and from 0 to 4.004 MeV for $^{122}$Sn. Using the one-step distorted-wave Born approximation (DWBA) analysis of the measured differential cross sections, we have identified spins and parities of 55 transitions to final states of $^{116}$Sn and to 63 transitions to final states of $^{122}$Sn. The $J^\pi$ values obtained have been compared with those reported in Ref. [6] for $^{116}$Sn and Ref. [7] for $^{122}$Sn, respectively, which summarize information on these nuclei obtained using different types of experimental measurements.

The excited states of $^{116}$Sn have been studied by a variety of methods that can be summarized as follows:

(i) Measurements of the energies of $\gamma$ rays following the $\beta^-$ decay of the $1^+$ ground state of $^{116}$In [8], and $\beta^+$ decays of the $3^+$ ground state of $^{116}$Sb and its $8^-$ isomer [9].

 

(ii) $^{115}$Sn$(n,\gamma)^{116}$Sn and $^{116}$Sn$(n,n'\gamma)^{116}$Sn experiments [10,11] which have identified 100 excited states, yielding unique spin assignments for more than half of them.
(iii) Nuclear resonance fluorescence techniques [12], which have determined level spins and parities from measurements of photon scattering cross sections, angular distributions, and linear polarizations or azimuthal asymmetries.
(iv) $^{114}$Cd$(\alpha,2n\gamma)$ studies, which have identified high-spin neutron quasiparticle excitations [13] as well as collective bands associated with $2p$-$2h$ excitations [14] up to levels with spin and parity $J^{\pi}=12^{+}$. The measurements included $\gamma$-ray excitation functions, $\gamma$-$\gamma$ coincidences, lifetimes, $\gamma$-ray angular distributions, $\gamma$-ray linear polarization, and conversion electron measurements.
(v) Neutron and $\alpha$-particle evaporation following fusion ($^{104}$Ru($^{18}$O,$\alpha 2n\gamma$) at 65 MeV [15]). The level scheme of $^{116}$Sn, previously known up to the 5388-keV $12^{+}$ level [13,14], was confirmed and extended to higher energies and spins.
(vi) Inelastic scattering of protons [16,17], deuterons [18], electrons [19], and Coulomb excitation [20,21].
(vii) One- and two-nucleon transfer reactions $^{115}$In($^{3}$He,$d$) [19], $^{115}$Sn$(d,p)$ [22], $^{115}$In$(\alpha,t)$ [19], $^{114}$Cd($^{3}$He,$n$) [23], $^{117}$Sn$(p,d)$ [24], $^{117}$Sn$(d,t)$ [22,25,26], $^{117}$Sn($^{3}$He,$\alpha$) [25], and $^{118}$Sn$(p,t)$ [5,27].

Among the methods used to study excited levels of $^{122}$Sn are the following:

(i) Spectroscopy of the $\gamma$ rays following the $\beta^{-}$ decay of the 1.5 s, 10.3 s, and 10.8 s isomeric states of $^{122}$In have been studied using different types of sources: an isotopically separated source from the $^{238}$U$(p,f)$ reaction followed by online isotope separation [28], a source produced via $^{124}$Sn$(d,\alpha)$ [28], a source from $^{235}$U$(n,f)$, isotopically and chemically separated [29], and a source produced via the $(n,p)$ reaction with 14-MeV neutrons on enriched samples of $^{122}$Sn [30].
(ii) Inelastic scattering of protons [16,31] and deuterons [18], and Coulomb excitation [20,21], including in-beam $\gamma$-ray spectroscopy using the $(n,n'\gamma)$reaction [32,33].
(iii) Nuclear resonance fluorescence experiments [12,34].
(iv) Identification of a long-lived $^{122}$Sn $10^{+}$ isomer (62 $\mu$s) among the products of $^{124}$Sn + $^{76}$Ge at 325 MeV [35].
(v) The $^{124}$Sn$(p,t)^{122}$Sn reaction. Subsequent to the study by Fleming *et al.* [5] referred to previously, there were measurements by Yagi *et al.* [36] and Kumabe *et al.* [31]. A study of the energy dependence of the $(p,t)$ reaction on $^{124}$Sn was carried out by Matoba *et al.* [37].
(vi) Alpha-cluster pickup via the $^{126}$Te$(d,^{6}$Li$)^{122}$Sn reaction at 33 MeV for states up to about 3.7 MeV of excitation energy [38], and very selective proton pickup via the $^{123}$Sb$(t,\alpha)^{122}$Sn reaction at incident triton energy of 12 MeV [39].

The results obtained in the studies mentioned above for $^{116,122}$Sn nuclei are reported in the Nuclear Data Sheets (NDS) compilations [6,7], where a more complete list of references can be found.

Along with the experimental work, we have also performed DWBA microscopic calculations of cross-section angular distributions for the ground state and some excited states of $^{116}$Sn and $^{122}$Sn nuclei, using two-neutron spectroscopic amplitudes derived from a shell-model study that includes the model space states with seniority less than or equal to 4. Full shell-model studies of both positive- and negative-parity spectra of $^{116}$Sn and $^{122}$Sn have been also performed.

The outline of the paper is as follows: The setup and the experiments are described in the next section, while the analysis of the experimental results is presented in Sec. III. Section IV is devoted to the results concerning the $^{118}$Sn$(p,t)^{116}$Sn and $^{124}$Sn$(p,t)^{122}$Sn reaction studies. In Sec. V we briefly outline the theoretical framework of our shell-model calculations and compare experimental and theoretical energy spectra of $^{116}$Sn and $^{122}$Sn nuclei. In Sec. VI we show how form factors are derived in the microscopic DWBA calculation and compare experimental and theoretical cross-section angular distributions. A summary of our study is given in Sec. VII.

## II. EXPERIMENTAL PROCEDURE

The $^{118}$Sn$(p,t)^{116}$Sn and $^{124}$Sn$(p,t)^{122}$Sn reaction measurements have been carried out at 24.6 and 25 MeV, respectively, using the unpolarized proton beam from the HVEC MP Tandem accelerator of the Maier-Leibnitz Laboratory of the Ludwig Maximilians University and Technical University of Munich.

The beam current intensity ranged from 200 to 350 nA to avoid target heating. The $^{118}$Sn target (isotopic enrichment 98.8%) had a thickness of 86 $\mu$g/cm$^2$ on a carbon backing of 7.5 $\mu$g/cm$^2$ while the $^{124}$Sn target (isotopic enrichment 96.71%) had a thickness of 80 $\mu$g/cm$^2$ on a carbon backing of 15 $\mu$g/cm$^2$. Thanks to the high isotopic enrichment of the targets, we measured triton spectra free of contributions from the different tin isotopes.

The reaction products have been analyzed with a Q3D magnetic spectrograph and detected in its focal plane.

The tritons emitted in the $^{118}$Sn$(p,t)^{116}$Sn reaction were identified by the new 1-m long focal plane detector, consisting of a proportional counter with cathode strip readout [40], designed to detect light ions like $p$, $d$, $t$, $^{3}$He, and alpha with a position resolution better than 0.1 mm, good particle identification, and high count rate. The particles were stopped in a 7-mm-thick plastic scintillator (NE-104). The photomultiplier signals together with the wire signals allowed the particle identification.

In the case of the $^{124}$Sn$(p,t)^{122}$Sn reaction measurements, we used the 1.8-m-long focal plane detector for light ions [41]. It consisted of an array of single-wire proportional detectors with an additional readout structure, followed by a rest energy plastic scintillator detector. This device provides position determination, focal plane reconstruction, and $\Delta E$-$E$ particle identification. As the tritons are very well separated from other reaction products, the resulting spectra are virtually free of contaminants. Thanks to the very good energetic characteristics

of the accelerator, the spectrograph, and the detectors, we were able to perform high-resolution measurements of triton spectra, about 8 keV full width at half maximum. The emitted tritons were detected at eight angles: In the case of $^{118}$Sn$(p,t)^{116}$Sn reaction between 10° and 55° and, in the case of $^{124}$Sn$(p,t)^{122}$Sn reaction between 6° and 52.5°, relative to the beam axis. Different magnetic field settings of the Q3D allowed us to reach excitation energies of 3.843 MeV in the $^{116}$Sn residual nucleus and 4.004 MeV in the $^{122}$Sn residual nucleus. The acceptance of the spectrograph was 11.04 msr, except for the most forward angles (6°), where it was 2.98 msr.

A Faraday cup behind the target integrated the beam current, allowing measurements of absolute differential cross sections. The uncertainties regarding the target thickness, solid angle, collected charge, and background subtraction at high excitation energies, give a systematic error of ∼15%.

The fitting procedure of triton spectra was carried out with the AUTOFIT shape-fitting code [42] using as reference the shape of the triton peak at 2.266 MeV for the $^{118}$Sn$(p,t)^{116}$Sn reaction and at 2.416 MeV for the $^{124}$Sn$(p,t)^{122}$Sn reaction. Areas and centroids of the triton peaks were determined.

The high resolving power of the spectrograph, the small background, the large solid angle, and the high spectrum energy resolution, allowed measurement of the cross sections of rather weakly populated levels. For instance, the $^{122}$Sn level at 2.530 MeV assigned as $(0)^+$ in the adopted level scheme [7], was identified in the 1.5 s $^{122}$In $\beta^-$ [29] and in $(n,n'\gamma)$ reaction studies [32,33]. It is populated in the present $(p,t)$ reaction with an integrated cross section (from 6° to 52.5°) of $(0.8 \pm 0.2)$ $\mu$b.

Absolute energy calibrations were constructed using known levels in each nucleus determined by $\gamma$ decay [6,7] and identified also in our $(p,t)$ experiments. The correlation between the measured channels and the excitation energies was established with a polynomial of rank 3 for the $^{124}$Sn$(p,t)^{122}$Sn reaction, measured with the long (1.8 m) detector and of rank 2 in the case of $^{118}$Sn$(p,t)^{116}$Sn reaction measured with the newer but shorter (1 m) detector. The parameters of the polynomials were fixed in the measured range by imposing the reproduction of the adopted energies. The achieved uncertainties in our quoted energies are estimated at 3 keV.

Figure 1 shows an example of the measured spectra of the two reactions. In these spectra, at $\theta = 20°$ for the $^{118}$Sn$(p,t)^{116}$Sn reaction and at $\theta = 15°$ for the $^{124}$Sn$(p,t)^{122}$Sn reaction, the excitation energies of the most prominent peaks are indicated.

We have studied 55 $(p,t)$ transitions to the final states of $^{116}$Sn up to $E_x = 3.843$ MeV, and 63 $(p,t)$ transitions to the final states of $^{122}$Sn up to $E_x = 4.004$ MeV.

The spins and parities of all the $^{116}$Sn and $^{122}$Sn levels have been assigned by the distorted-wave Born approximation (DWBA) analysis reported in Sec. III.

Tables I and II report the spectroscopic information on $^{116}$Sn and $^{122}$Sn deduced from the present transfer reaction experiments, compared with information available in the literature [6,7]. The last column of each table reports the experimental cross sections integrated from 10° to 55° for the $^{118}$Sn$(p,t)^{116}$Sn reaction and from 6° to 52.5° for the $^{124}$Sn$(p,t)^{122}$Sn reaction and the corresponding statistical errors.

These tables are relevant to the need for a large body of data to test and confirm nuclear structure models. They are also relevant to the question of the completeness of the spectroscopic information provided by different reactions. For example, neutron capture and fusion reactions are generally regarded as providing a more complete picture of the spectrum of a daughter nucleus than does the more selective $(p,t)$ reaction. However, in the present $(p,t)$ experiment we have identified 38 levels below the excitation energy of 3.5 MeV in both $^{116}$Sn and $^{122}$Sn. This is the same number of levels identified below 3.5 MeV in $^{116}$Sn by Raman *et al.* [10] using $(n,\gamma)$ and $(n,n'\gamma)$ reactions, and only one fewer than the number of levels identified below 3.5 MeV in $^{122}$Sn by Demidov and Mikhailov [32] and Govor *et al.* [33] using the $(n,n'\gamma)$ reaction. This shows that the $(p,t)$ reaction is not less effective than $(n,\gamma)$ or $(n,n'\gamma)$ in identifying most of the levels of a daughter nucleus, when the high-resolution measurement allows one to identify also very weakly excited levels.

## III. DATA ANALYSIS

To determine the value of the transferred angular momentum and spin for each level in the final nuclei $^{116}$Sn and $^{122}$Sn, we compared the experimental angular distributions with the predictions of cluster DWBA calculations.

In the case of a $(p,t)$ reaction on a $0^+$ initial state, and assuming that the two neutrons are transferred in a one-step process in a relative $L = 0$ state and in a pure singlet $(S = 0)$ space-symmetric $s$ state, only natural-parity states in the residual nucleus are populated. The $J^\pi$ of the final states can be inferred by $L$-transfer identification $[J_f = L, \pi_f = (-1)^L]$.

The most fully studied case of $(p,t)$ from a $0^+$ state to an unnatural parity level is the $^{208}$Pb$(p,t)^{206}$Pb transition to a $3^+$ level at 1340.5 keV. This was a subject of considerable interest in the late 1970s and early 1980s. Nagarajan, Strayer, and Werby [43] were able to account for the transition as a one-step process by including the exact wave function of the triton and the fact that the proton interacts individually with the two neutrons (not just with their mass center). Igarashi and Kubo [44] considered the contribution from sequential transfer $[(p,d) + (d,t)]$. No universal agreement was reached about the relative importance of the different mechanisms that can contribute to a $(p,t)$ transition from a $0^+$ state to an unnatural parity level, but there can be no doubt that such transitions occur.

DWBA analyses of the differential cross sections for the $^{118,124}$Sn$(p,t)^{116,122}$Sn reactions have been performed, assuming a semimicroscopic dineutron cluster pickup. Our DWBA analysis is along the same lines of those carried out in the case of $^{114}$Sn [2], $^{110}$Sn [1], and $^{118}$Sn [3]: Basically we assumed that the relative motion of the transferred spin-singlet neutron pair has zero angular momentum and no radial nodes. We describe the center-of-mass wave function of the transferred neutron pair by a single-particle wave function with angular momentum equal to the total angular momentum

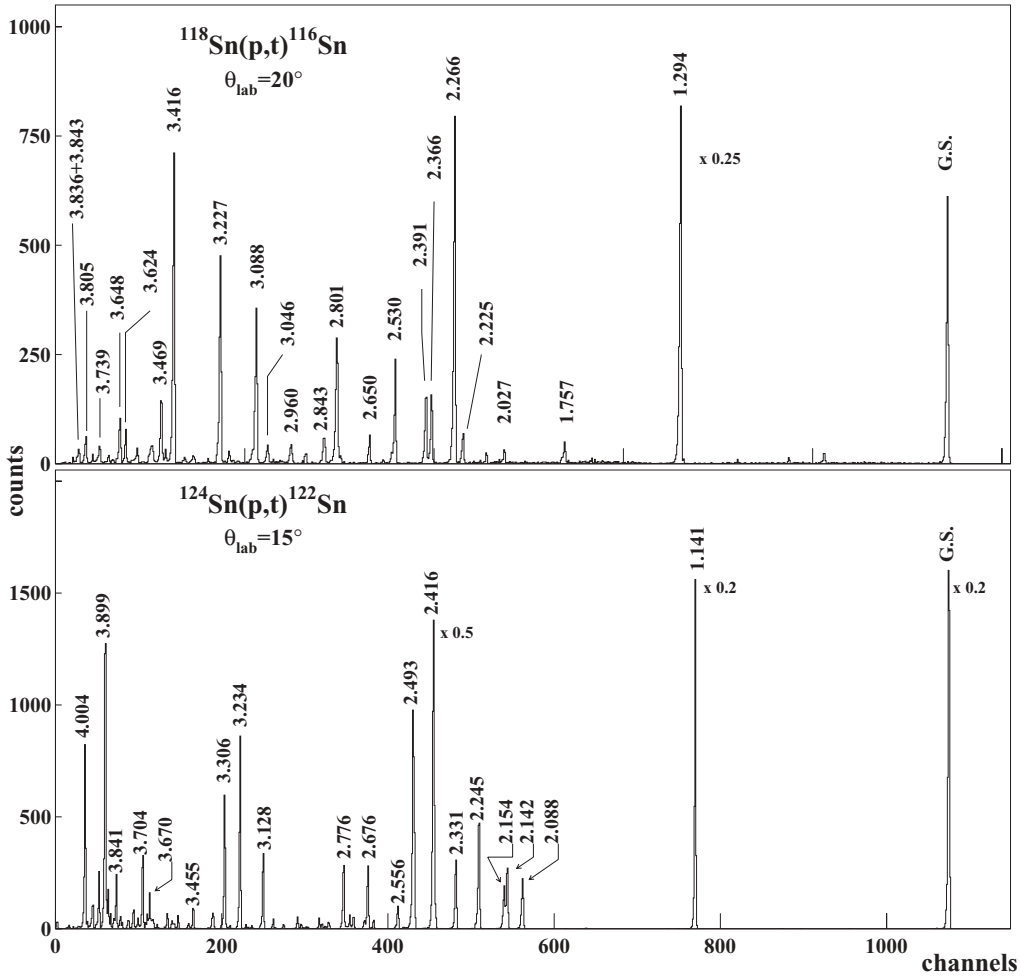


FIG. 1. Position spectrum of tritons measured at $\theta = 20^\circ$ for the $^{118}$Sn$(p,t)^{116}$Sn reaction, and at $\theta = 15^\circ$ for the $^{124}$Sn$(p,t)^{122}$Sn reaction. Some levels are labeled with their excitation energy in MeV.

$L$ of the transferred pair. The number $N$ of nodes in the radial bound-state wave function of the center of mass is given by the conservation rule for three-dimensional harmonic oscillator quanta:

$$Q = 2N + L = \sum_{i=1}^{2}(2n_i + \ell_i),$$

where $n_i$ and $l_i$ are the quantum numbers of the individual shell-model states that form the transferred pair. This prescription may be ambiguous when the dineutron pair is composed of shell-model orbitals from different major oscillator shells. However, the calculated angular distributions are determined mainly by $L$ and are only slightly affected if $N$ changes by one, and consequently this ambiguity in $N$ presents little effect on our conclusions. The shapes of the angular distributions depend very little on the detailed microscopic shell-model components of the transferred dineutron pair and for these reasons the DWBA calculations are a valuable guide in the use of the observed angular distributions to extract the transferred angular momentum $L$. On the contrary, the detailed shell-model structure of the dineutron pair is important in determining the magnitude of the differential cross sections (i.e., the $n_i$ and $l_i$ values of the components of the cluster) and the relative phases with which these components appear in the cluster. This will be shown in the description in Sec. V of our shell-model calculations of the spectroscopic amplitudes and in Sec. VI where these amplitudes are used together with the DWBA to obtain absolute cross sections for $(p,t)$ reactions on $^{118}$Sn and $^{124}$Sn.

The cluster DWBA calculations have been performed in finite range approximation, using the computer code TWOFNR [45] and proton-dineutron interaction potential of the Gaussian form $V(r_{p2n}) = V_0\exp[-(r_{p2n}/\xi)^2]$ with $\xi = 2$ fm. The optical model parameters for the proton entrance channel have been deduced from a systematic survey of elastic scattering by Perey [46], for the triton exit channel by Fleming *et al.* [5] and have been slightly adjusted for an optimized agreement with the experimental angular distributions.

In Table III the optical model parameters for the proton and triton continuum wave functions, and the geometrical parameters used for evaluating the bound-state wave functions of the transferred dineutron cluster are reported. By means of the same set of optical model parameters we have analyzed the

TABLE I. Columns 1 and 2 give the $^{116}$Sn adopted energies, spins, and parities; columns 3 and 4 the energies, spins, and parities observed in the present work; column 5 gives the integrated cross sections from 10° to 55°. Our energies have an uncertainty of ±3 keV. In column 5 integrated cross sections, estimated with a systematic error of ±15%, are reported together with the statistical errors.

| $^{116}$Sn Level scheme | | | | |
|---|---|---|---|---|
| Adopted | | Present experiment | | |
| $E_{exc}$ (keV) | $J^\pi$ | $E_{exc}$ (MeV) | $J^\pi$ | $\sigma_{int}$ ($\mu$b) |
| 0.0 | $0^+$ | 0.000 | $0^+$ | 1345±24 |
| 1293.560 | $2^+$ | 1.294 | $2^+$ | 433±13 |
| 1756.864 | $0^+$ | 1.757 | $0^+$ | 39±1 |
| 2027.48 | $0^+$ | 2.027 | $0^+$ | 17±1 |
| 2112.323 | $2^+$ | 2.112 | $2^+$ | 2.5±0.4 |
| 2225.379 | $2^+$ | 2.225 | $2^+$ | 8±1 |
| 2266.159 | $3^-$ | 2.266 | $3^-$ | 165±3 |
| 2365.975 | $5^-$ | 2.366 | $5^-$ | 59±2 |
| 2390.879 | $4^+$ | 2.391 | $4^+$ | 52±2 |
| 2529.202 | $4^+$ | 2.530 | $4^+$ | 71±2 |
| 2545.71 | $(0^+)$ | 2.546 | $0^+$ | 3.6±0.4 |
| | | 2.585 | $1^-$ | 1.5±0.3 |
| 2585.564 | $1^+$ | | | |
| 2650.438 | $2^+$ | 2.650 | $2^+$ | 8±1 |
| 2773.33 | $6^-$ | | | |
| 2790.55 | $(0)^+$ | 2.790 | $4^+$ | 6±1 |
| 2801.28 | $4^+$ | 2.801 | $4^+$ | 152±3 |
| 2843.82 | $2^+$ | 2.843 | $2^+$ | 11±1 |
| 2908.85 | $7^-$ | 2.907 | $7^-$ | 18±1 |
| 2960.03 | $2^+$ | 2.960 | $2^+$ | 8±1 |
| 2996.27 | $3^+$ | | | |
| 3016.44 | $6(^-)$ | | | |
| 3032.70 | $6^+$ | | | |
| 3046.40 | $4^+$ | 3.046 | $4^+$ | 13±1 |
| 3088.63 | $2^+$ | 3.088 | $2^+$ | 48±2 |
| 3096.93 | $4^+$ | 3.096 | $4^+$ | 16±1 |
| 3105.18 | $5^-$ | 3.105 | $5^-$ | 6±1 |
| 3157.73 | $3^-$,4 | 3.157 | $4^+$ | 2.2±0.4 |
| 3179.68 | $3^+$ | | | |
| 3184 | $3^-$ | 3.179 | $3^-$ | 2.5±0.4 |
| 3194.32 | $0^+$ | 3.194 | $0^+$ | 15±1 |
| 3210.00 | $7^-$ | 3.210 | $7^-$ | 2.0±0.3 |
| 3227.45 | $(2^+)$ | 3.227 | $2^+$ | 62±2 |
| 3227.95 | $8^-$ | | | |
| 3228.06 | $2^+$ | 3.231 | $2^+$ | 6±1 |
| 3236.02 | $0^+$ | | | |
| | | 3.251 | $6^+$ | 1.5±0.3 |
| 3257.67 | $3^-$,$4^-$,$5^-$ | | | |
| 3277.6 | $6^+$ | | | |
| | | 3.278 | $4^+$ | 4.0±0.5 |
| 3288.99 | LE 4 | | | |
| 3309.0 | $6^-$ | | | |
| 3314.99 | $3^+$ | | | |
| 3333.78 | $1^-$ | 3.333 | $1^-$ | 5±1 |
| | | 3.344 | $5^-$ | 3.0±0.4 |
| 3344.34 | $2^+$ | | | |
| 3350.5 | $(5^+)$ | | | |
| | | 3.371 | $3^-$ | 3.1±0.4 |
| 3371.42 | $3^+$ | | | |
| 3379.8 | $3^+$ | | | |
| 3416.2 | $2^+$ | 3.416 | $2^+$ | 92±2 |
| 3427.91 | $4^-$ | | | |
| 3453.2 | 4,5 | | | |
| | | 3.453 | $3^-$+$5^-$ | 9±1 |
| 3469.61 | $2^+$ | 3.469 | $2^+$ | 26±1 |
| 3492.98 | $8^+$ | | | |
| | | 3.493 | $7^-$ | 2.3±0.3 |
| 3507.25 | $5^-$ | | | |
| 3508.33 | $2^+$ | | | |
| 3510 | $4^+$ | 3.506 | $4^+$ | 20±1 |
| 3513.6 | $(2)^+$ | 3.514 | $4^+$ | 8±1 |
| 3522.66 | $9^-$ | 3.522 | $9^-$ | 6±1 |
| 3547.16 | $10^+$ | | | |
| | | 3.549 | $(8^+,9^-)$+$3^-$ | 2.0±0.3 |
| 3551.7 | $3^+$ | | | |
| 3572.77 | $2^+$,3 | 3.572 | $3^-$ | 7±1 |
| 3576.2 | 4+,5 | | | |
| 3586.63 | $2^+$ | 3.586 | $2^+$ | 1.7±0.3 |
| 3593.76 | $3^+$ | | | |
| 3616.3 | $4^-$ | | | |
| 3624.6 | $4^+$ | 3.624 | $4^+$ | 23±1 |
| 3640.7 | $4,5^+$ | | | |
| | | 3.648 | $6^+$ | 55±2 |
| 3648.1 | $3^-$,$5^-$ | | | |
| 3658.05 | $2^+$ | | | |
| | | 3.679 | $7^-$ | 7±1 |
| | | 3.699 | $1^-$ | 4.2±0.5 |
| 3706.9 | $3^+$ | | | |
| 3711.89 | $(1)^+$ | | | |
| | | 3.712 | $7^-$ | 1.9±0.3 |
| 3712.4 | $8^+$ | | | |
| | | 3.724 | $0^+$ | 2.1±0.3 |
| 3730.6 | LE 3 | | | |
| 3739 | $3^+$ | | | |
| | | 3.739 | $6^+$ | 26±1 |
| 3742.90 | $3^-$ | 3.747 | $3^-$ | 4.5±0.5 |
| 3747.9 | LE 3 | | | |
| | | 3.771 | $4^+$ | 4.7±0.5 |
| 3776.78 | $1^+$ | | | |
| 3787.2 | $(6^-)$ | | | |
| 3797 | $^+$ | | | |
| 3805.5 | $4^+$ | | | |
| | | 3.805 | $4^+$+$2^+$ | 12±1 |
| 3806.02 | $2^+$ | | | |
| 3809.3 | $2^+$,3 | | | |
| 3836.67 | $0^+$ | 3.836 | $0^+$ | 11±1 |
| 3843.66 | $2^+$,3 | 3.843 | $2^+$ | 2.2±0.4 |

angular distributions of $^{112,116,120,122}$Sn($p$,$t$) reactions [1–4], and $^{121,123}$Sb($p$,$t$) reactions [47,48] achieving good agreement between experimental results and DWBA calculations, and therefore supporting the assumption that two-step processes, not taken into account, are small in this mass region.

The experimental data and the results of the calculations for different $L$ transfers are compared in Figs. 2–7

TABLE II. Columns 1 and 2 give the $^{122}$Sn adopted energies, spins, and parities; columns 3 and 4 the energies, spins, and parities observed in the present work; column 5 gives the integrated cross sections from 6° to 52.5°. Our energies have an uncertainty of ±3 keV. In column 5 integrated cross sections, estimated with a systematic error of ±15%, are reported together with the statistical errors.

| $^{122}$Sn Level scheme | | | | |
|---|---|---|---|---|
| Adopted | | Present experiment | | |
| $E_{exc}$ (keV) | $J^\pi$ | $E_{exc}$ (MeV) | $J^\pi$ | $\sigma_{int}$ ($\mu$b) |
| 0.0 | $0^+$ | 0.0 | $0^+$ | 958±15 |
| 1140.51 | $2^+$ | 1.141 | $2^+$ | 370±10 |
| 2087.71 | $0^+$ | 2.088 | $0^+$ | 28±1 |
| 2142.06 | $4^+$ | 2.142 | $4^+$ | 43±2 |
| 2153.81 | $2^+$ | 2.154 | $2^+$ | 14±1 |
| 2245.81 | $5^-$ | 2.245 | $5^-$ | 148±3 |
| 2331.09 | $4^+$ | 2.331 | $4^+$ | 69±2 |
| 2409.03 | $7^-$ | 2.409 | $7^-$ | 66±2 |
| 2415.543 | $2^+$ | 2.416 | $2^+$ | 187±3 |
| 2492.67 | $3^-$ | 2.493 | $3^-$ | 171±3 |
| 2530.33 | $(0)^+$ | 2.530 | $0^+$ | 0.8±0.2 |
| 2555.42 | $6^+$ | 2.556 | $6^+$ | 14±1 |
| 2651.37 | $4^-,5^-,6^-$ | | | |
| 2653.00 | $6^-$ | | | |
| | | 2.654 | $6^+ + 4^+$ | 6±1 |
| 2657 | | | | |
| 2675.57 | $0^+$ | 2.676 | $0^+$ | 47±2 |
| 2690.04 | $(8^+)$ | 2.690 | $7^-$ | 8±1 |
| 2734.50 | $2^+$ | 2.735 | $2^+$ | 4±1 |
| 2751.01 | $5^-$ | 2.752 | $5^-$ | 15±1 |
| 2765.6 | $(10^+)$ | 2.766 | $6^+$ | 4±1 |
| 2775.55 | $2^+$ | 2.776 | $2^+$ | 17±1 |
| 2837.88 | $6^-$ | | | |
| | | 2.838 | $6^+$ | 8±1 |
| | | 2.855 | $4^+$ | 2.1±0.4 |
| 2855.47 | $4^-$ | | | |
| 2867.73 | | 2.868 | $0^+$ | 4±1 |
| 2879.79 | $1^+,2^+$ | | | |
| | | 2.880 | $1^-$ | 2.4±0.5 |
| 2944.96 | $3^+$ | | | |
| 2959.12 | $4^+$ | | | |
| | | 2.960 | $2^+$ | 1.6±0.3 |
| 2971.1 | | | | |
| 2973.39 | $4^+$ | 2.973 | $4^+$ | 10±1 |
| 3035.91 | $3^-$ | 3.036 | $3^-$ | 2.2±0.4 |
| | | 3.072 | $4^+$ | 1.1±0.3 |
| 3082.15 | $4^+$ | 3.082 | $4^+$ | 8±1 |
| 3128.6 | $2^+$ | 3.128 | $2^+$ | 23±1 |
| 3130.58 | | | | |
| 3206.25 | $(0)^+$ | 3.206 | $0^+$ | 5±1 |
| 3233.74 | $4^+$ | 3.234 | $4^+$ | 158±3 |
| 3281.43 | | | | |
| | | 3.282 | $5^-$ | 2.2±0.4 |
| 3305.69 | $4^+$ | 3.306 | $4^+$ | 110±3 |
| 3330 | | | | |
| 3358.59 | $1^-$ | 3.358 | $1^-$ | 7±1 |
| 3362.87 | $3^-$ | 3.364 | $3^-$ | 5±1 |
| 3371.24 | $(2^+)$ | | | |
| 3416.5 | $(7^-,8^-,9^-)$ | | | |
| 3454.82 | $(3^-)$ | 3.455 | $3^-$ | 11±1 |
| 3478.60 | $(7^-)$ | 3.478 | $4^+$ | 3±1 |
| 3530.71 | $(7^-,8^-)$ | 3.529 | $4^+$ | 12±1 |
| 3548.66 | $2^+$ | | | |
| 3568.14 | | | | |
| 3582.35 | $2^+$ | 3.583 | $2^+$ | 5 ± 1 |
| 3627.01 | $4^+$ | 3.627 | $4^+$ | 3 ± 1 |
| | | 3.653 | $2^+$ | 4 ± 1 |
| | | 3.661 | $4^+$ | 10 ± 1 |
| 3670.28 | $4^+$ | 3.670 | $4^+$ | 28 ± 1 |
| | | 3.683 | $3^-$ | 7 ± 1 |
| | | 3.692 | $2^+$ | 1.2 ± 0.3 |
| 3703.38 | $(7^-,8^-,9^-)$ | | | |
| | | 3.704 | $2^+ + 7^-$ | 30 ± 1 |
| 3704.9 | $(2^+)$ | | | |
| 3710.15 | $(7^-,8^-)$ | | | |
| 3730.00 | | | | |
| | | 3.731 | $3^-$ | 6 ± 1 |
| 3751.3 | $2^+$ | 3.752 | $2^+$ | 6 ± 1 |
| | | 3.758 | $6^+$ | 1.7 ± 0.3 |
| 3758.51 | $1,2^+$ | | | |
| | | 3.775 | $5^-$ | 4 ± 1 |
| 3777.0 | | | | |
| 3782.84 | $(4^+)$ | 3.783 | $2^+$ | 3 ± 1 |
| 3810 | + | 3.810 | $4^+$ | 9 ± 1 |
| 3818 | $(6^+)$ | | | |
| 3819.79 | $2^+$ | 3.820 | $2^+$ | 2.7 ± 0.4 |
| 3840.65 | $(4^+)$ | 3.841 | $4^+$ | 39 ± 2 |
| | | 3.855 | $3^-$ | 2.8 ± 0.4 |
| | | 3.871 | $5^-$ | 13 ± 1 |
| 3871.1 | $1,2^+$ | | | |
| 3876.53 | $5^-,6^+$ | | | |
| 3882.10 | $4^+$ | 3.882 | $4^+$ | 32 ± 1 |
| 3899.68 | $0^+,1^+,2^+$ | 3.899 | $2^+$ | 91 ± 2 |
| 3900 | | | | |
| 3929.9 | $1,2^+$ | 3.930 | $2^+$ | 14 ± 1 |
| 3948.5 | $5^-,6^+$ | | | |
| 3974 | | 3.966 | $5^-$ | 20 ± 1 |
| 4004.0 | $(2^+)$ | 4.004 | $2^+$ | 44 ± 2 |

for the $^{118}$Sn$(p,t)^{116}$Sn reaction and in Figs. 8–13 for the $^{124}$Sn$(p,t)^{122}$Sn reaction. The clear structure of the angular distributions, allowing easy discrimination among different $L$ transfers, is well described by the DWBA calculations (Fig. 14).

For all the doublets observed in $^{118}$Sn$(p,t)^{116}$Sn and $^{124}$Sn$(p,t)^{122}$Sn reactions, the percentage of the two different $L$ contributions have been determined minimizing the $\chi^2$ of the fit to the angular distribution.

## IV. RESULTS

### A. $^{118}$Sn$(p,t)^{116}$Sn reaction

As Table I shows, with respect to the adopted levels (NDS) [6], 32 assignments have been confirmed, seven ambiguities removed, 13 new levels have been for the first time observed and identified in $J^\pi$. Three unresolved doublets have been

TABLE III. The Woods-Saxon optical model parameters for the incident proton, the outgoing triton, and the geometrical parameters for the bound state (BS) of the transferred dineutron cluster.

| | $V_r$ (MeV) | $r_r$ (fm) | $a_r$ (fm) | $W_v$ (MeV) | $r_v$ (fm) | $a_v$ (fm) | $W_d$ (MeV) | $r_d$ (fm) | $a_d$ (fm) | $V_{so}$ (MeV) | $r_{so}$ (fm) | $a_{so}$ (fm) | $r_c$ (fm) |
|---|---|---|---|---|---|---|---|---|---|---|---|---|---|
| $p$ | 50.0 | 1.25 | 0.65 | | | | 10.0 | 1.30 | 0.60 | 3.00 | 1.25 | 0.70 | 1.25 |
| $t$ | 176.0 | 1.14 | 0.72 | 18.0 | 1.61 | 0.82 | | | | 8.00 | 1.10 | 0.80 | 1.30 |
| BS | | 1.30 | 0.50 | | | | | | | | | | |

observed, giving two confirmations, two new assignments, one tentative assignment, and one removed ambiguity.

The proposed assignments for the levels observed in the present measurements of $^{118}$Sn$(p,t)^{116}$Sn reaction, new or corresponding to those reported in the NDS [6] with uncertain $J^\pi$ or without $J^\pi$ assignment, are discussed in the following, together with the unresolved doublets.

*2.546 MeV.* The adopted level scheme [6] reports a level at 2545.71 keV with $J^\pi = (0^+)$ identified in Coulomb excitation [20,21], $(n,n'\gamma)$ [10,11], $(n,\gamma)$ [10] reactions, and isomeric radioactive decays [8,9]. In our $(p,t)$ measurement the angular distribution of the 2.546 MeV level is quite well reproduced by $L=0$ transfer. Present assignment $J^\pi = 0^+$ removes the uncertainty in the NDS assignment.

*2.585 MeV.* In Ref. [6] a level at 2585.564 keV is given on the basis of $(n,n'\gamma)$ [10,11], $(n,\gamma)$ [10], $(d,t)$, and $(^3$He,$\alpha)$ [22,25] and $(p,p')$ [16,17] with $1^+$ assignment. In our measurement is observed a weakly populated level at 2.585 MeV. The shape of its angular distribution is well reproduced by an $L=1$ transfer. Present assignment $J^\pi = 1^-$.

*2.790 MeV.* In the adopted level scheme [6], a level is listed at 2790.55 keV with $J^\pi=(0)^+$, deduced from $(n,n'\gamma)$ study [10]. In the present experiment the angular distribution does not display the characteristic $L$=0 transfer shape, while an $L$=4 transfer reasonably reproduces the differential cross section. Present assignment $J^\pi = 4^+$.

*3.157 MeV.* The NDS [6] report a level at 3157.73 keV observed in $(n,n'\gamma)$ [10,11], $(n,\gamma)$ [10] with $J^\pi = 3^-$, 4. In the present experiment an $L=4$ transfer reproduces the measured angular distribution fairly well and it is consistent with an assignment of $J^\pi = 4^+$.

*3.227 MeV, 3.231 MeV.* In the adopted level scheme [6] are reported levels at 3227.45, 3227.95, and 3228.06 keV, with $J^\pi = (2^+)$, $8^-$, $2^+$ respectively. The first and the third level are identified from $(n,n'\gamma)$ [10,11], $(n,\gamma)$ [10] the second one in $^{114}$Cd$(\alpha,2n\gamma)$ [13], $^{115}$In$(\alpha,t\gamma)$ [49], and $^{104}$Ru$(^{18}$O,$\alpha 2n\gamma)$ [15]. In the present experiment, an $L=2$ transfer reasonably

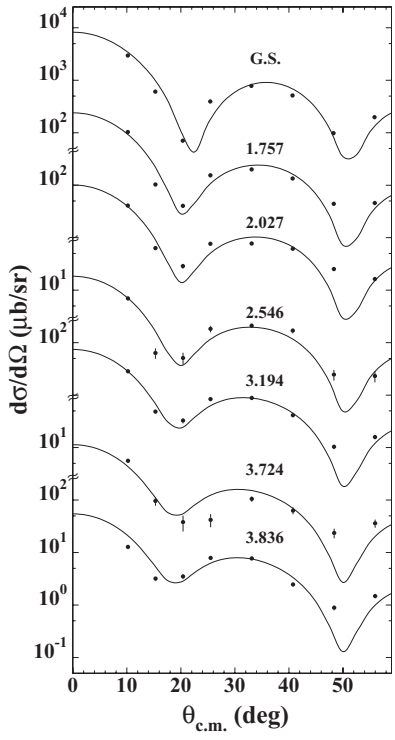


FIG. 2. Differential cross sections for the excitation of $0^+$ states by the $^{118}$Sn$(p,t)^{116}$Sn reaction. The dots represent the experimental data, and the solid lines the theoretical estimates obtained with semimicroscopic DWBA calculations. The energies attributed to the observed levels are those given in the present work.

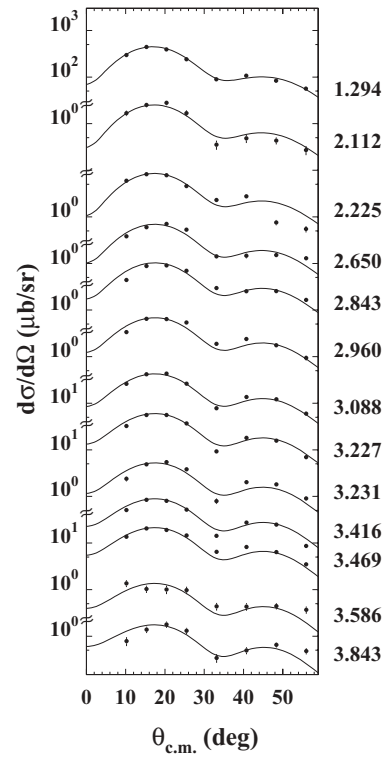


FIG. 3. Differential cross sections for the excitation of $2^+$ states by the $^{118}$Sn$(p,t)^{116}$Sn reaction. See Fig. 2 for details.

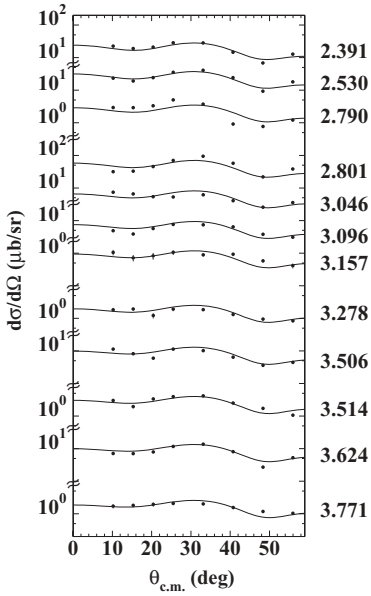


FIG. 4. Differential cross sections for the excitation of $4^+$ states by the $^{118}$Sn$(p,t)^{116}$Sn reaction. See Fig. 2 for details.

well reproduces the measured differential cross sections of the two levels at 3.227 and 3.231 MeV. Our present assignment is $J^\pi = 2^+$ both for the 3.227-MeV level, that coincides with the 3227.45-keV level, and for the 3.231-MeV level, that corresponds to the 3228.06-keV level reported on NDS compilation [6]. Our present assignment of $J^\pi = 2^+$ to the 3.227-MeV level removes the ambiguity in the NDS compilation [6].

*3.251 MeV.* No level is reported in the adopted level scheme [6] at this energy. In our experiment this level is weakly populated. The measured angular distribution is consistent with an attribution of $J^\pi = 6^+$.

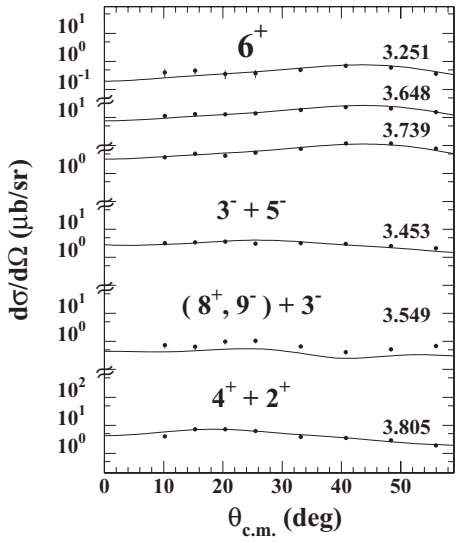


FIG. 5. Differential cross sections for the excitation of $6^+$ states and three doublets at 3.453, 3.549, and 3.805 MeV by the $^{118}$Sn$(p,t)^{116}$Sn reaction. See Fig. 2 for details.

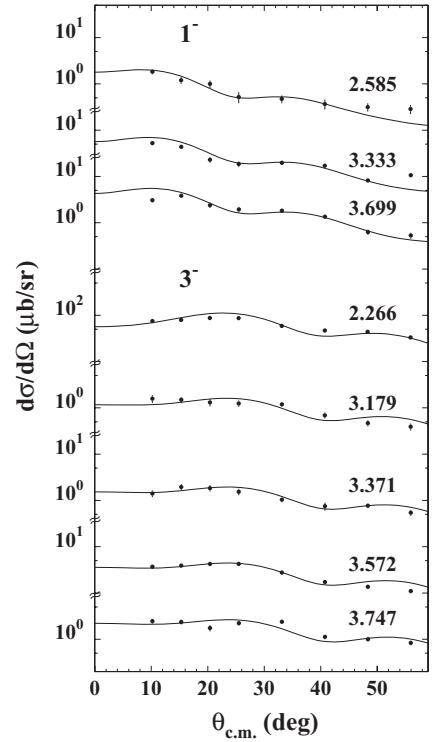


FIG. 6. Differential cross sections for the excitation of $1^-$ and $3^-$ states by the $^{118}$Sn$(p,t)^{116}$Sn reaction. See Fig. 2 for details.

*3.278 MeV.* A level at 3277.6 keV with $J^\pi = 6^+$ is reported on the adopted level scheme [6] from the measurement of $(\alpha,2n\gamma)$ [13], $(n,n'\gamma)$ [10,11], $(\alpha,t\gamma)$, ($^3$He,$d$), and $(\alpha,t)$ [19]. The measured angular distribution of the tritons populating the 3.278-MeV level is accurately reproduced by an $L = 4$ transfer. The present assignment is $J^\pi = 4^+$.

*3.344 MeV.* In the present experiment, the angular distribution of the tritons weakly populating the level at 3.344 MeV is reasonably well reproduced by an $L = 5$ transfer. The present assignment is therefore $J^\pi = 5^-$. This level is distinct from the adopted $J^\pi = 2^+$ level at 3344.34 keV, observed in $(n,n'\gamma)$ and $(n,\gamma)$ [10,11] and $^{115}$Sn$(d,p)$ [22].

*3.371 MeV.* In the NDS compilation [6], a level is given at an energy of 3371.42 keV with $J^\pi = 3^+$, deduced from $(n,n'\gamma)$,$(n,\gamma)$ [10,11] and $^{116}$Sb $\epsilon$ decay (15.8 min) studies [9]. In our study a level at very near energy, 3.371 MeV, is weakly populated and the differential cross section is quite well reproduced by $L = 3$ transfer. Present assignment $J^\pi = 3^-$.

*3.453 MeV.* In the adopted level scheme [6], a level is listed at 3453.2 keV with $J = 4,5$. In the present experiment, the rather featureless angular distribution is accurately reproduced by considering an unresolved doublet with $J^\pi = 3^-$ (50%) and $J^\pi = 5^-$ (50%).

*3.493 MeV.* The spin and parity reported in NDS [6] for the level at 3492.98 keV are $8^+$ deduced from $^{114}$Cd$(\alpha,2n\gamma)$ [13,14], $^{115}$In$(\alpha,t\gamma)$ [49], and $^{104}$Ru($^{18}$O,$\alpha 2n\gamma$) [15] studies. In our measurement an $L = 7$ transfer reasonably reproduces the angular distribution, while an $L = 8$ transfer overpredicts the experimental values starting from $\theta = 50^\circ$, as shown in

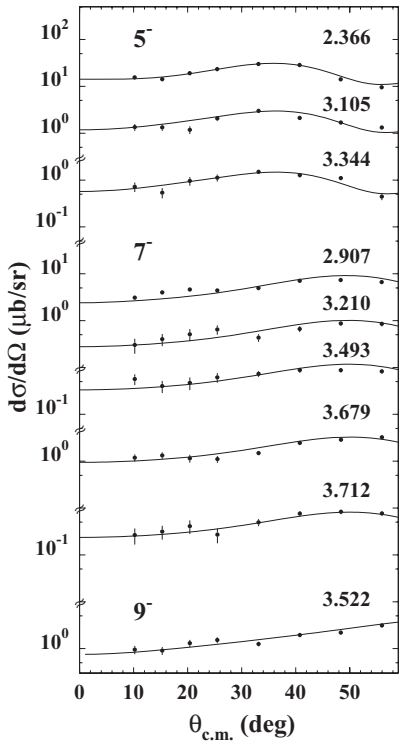


FIG. 7. Differential cross sections for the excitation of $5^-$, $7^-$, and $9^-$ states by the $^{118}$Sn$(p,t)^{116}$Sn reaction. See Fig. 2 for details.

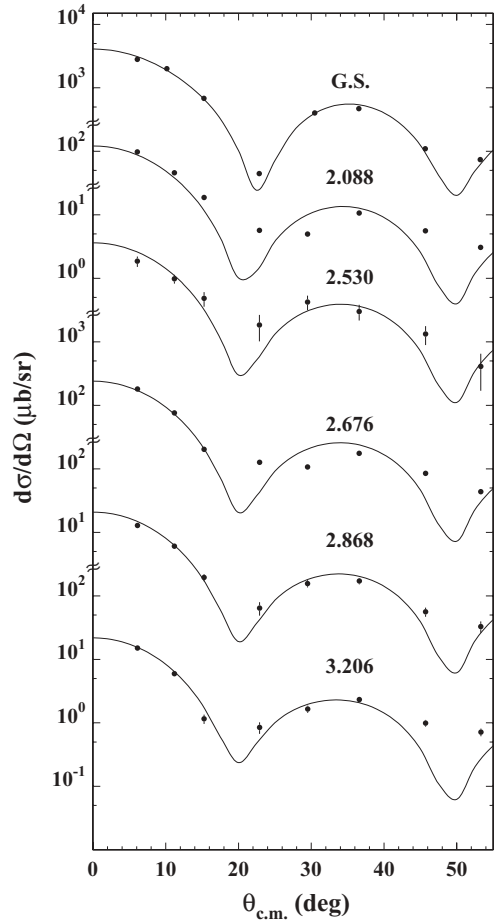


FIG. 8. Differential cross sections for the excitation of $0^+$ states by the $^{124}$Sn$(p,t)^{122}$Sn reaction. See Fig. 2 for details.

Fig. 15. The level we find at 3.493 MeV does not coincide with the adopted 3492.98-keV level. Present assignment $J^\pi = 7^-$.

*3.514 MeV.* In Ref. [6], a level is denoted with an energy of 3513.6 keV and $J^\pi = (2)^+$, deduced from $(n,\gamma)$ [10] and $^{117}$Sn$(d,t)$ [25] studies. In the present study, the angular distribution is compatible with an $L = 4$ transfer. Present assignment $J^\pi = 4^+$ removes the ambiguity in the NDS assignment.

*3.549 MeV.* In the adopted level scheme [6], two close levels are reported, the first at 3547.16 keV with $J^\pi = 10^+$ observed in $^{114}$Cd$(\alpha,2n\gamma)$ [13,14], and $^{104}$Ru$(^{18}$O$,\alpha 2n\gamma)$ [15] reactions and the second at 3551.7 keV with $J^\pi = 3^+$ deduced from $(n,n'\gamma)$, $(n,\gamma)$ [10,11] reaction studies. In our study this transition is weakly populated and the angular distribution can be well reproduced by considering an unresolved doublet with either $J^\pi = 8^+$ (70%) or $J^\pi = 9^-$ (70%) and $J^\pi = 3^-$ (30%), as shown in Fig. 16. Present tentative assignment $(8^+,9^-)$ + $3^-$.

*3.572 MeV.* The spin and parity reported in NDS [6] for the level at 3572.77 keV is $J^\pi = 2^+$, 3 inferred from a study of $(n,\gamma)$ reaction [10]. We identified a level at 3.572 MeV with an angular distribution well reproduced by an $L = 3$ transfer. Present assignment $J^\pi = 3^-$.

*3.648 MeV.* The 3648.1-keV level, reported in NDS [6], was assigned $3^-, 5^-$ by Raman *et al.* [10]. In the present experiment the 3.648-MeV state shows a clear $L = 6$ cross-section angular distribution. Present assignment $J^\pi = 6^+$.

*3.679 MeV.* No level is reported in the NDS compilation [6] at this energy. In our experiment, the angular distribution of the cross section to the level at 3.679 MeV is accurately reproduced by an $L = 7$ transfer. Present assignment $J^\pi = 7^-$.

*3.699 MeV.* The NDS [6] do not report a level at this energy. The measured differential cross section is consistent with an attribution of $J^\pi = 1^-$.

*3.712 MeV.* The NDS [6] report a level at 3711.89 keV with $J^\pi = (1)^+$, inferred from $(n,n'\gamma)$, $(n,\gamma)$ [10] reaction studies and a level at 3712.4 keV with $J^\pi = 8^+$ derived from $^{114}$Cd$(\alpha,2n\gamma)$ [13], $^{115}$In$(\alpha,t\gamma)$ [49], and $^{104}$Ru$(^{18}$O$,\alpha 2n\gamma)$ [15] studies. In the present $(p,t)$ measurement, the level is weakly populated and an $L = 7$ transfer reasonably reproduces the angular distribution. We assign $J^\pi = 7^-$ to this level, which probably does not coincide with either of the two levels reported in NDS.

*3.724 MeV.* The adopted level scheme [6] gives no level at this energy. In our measurement, the weakly populated 3.724-MeV level angular distribution displays a characteristic $L = 0$ transfer shape, with a very steeply rising cross section at very small reaction angles and a sharp minimum at the detector angle of about 20°. Present assignment $J^\pi = 0^+$.

*3.739 MeV.* The adopted level scheme [6] reports a level at 3739 keV with $J^\pi = 3^+$ inferred from $^{115}$In$(\alpha,t\gamma)$, $(^3$He$,d)$ [49], and $^{117}$Sn$(d,t)$ [26] studies. In our measurement the angular distribution of the 3.739-MeV level, which probably does not correspond to the adopted one, is well reproduced by an $L = 6$ transfer. Present assignment $J^\pi = 6^+$.

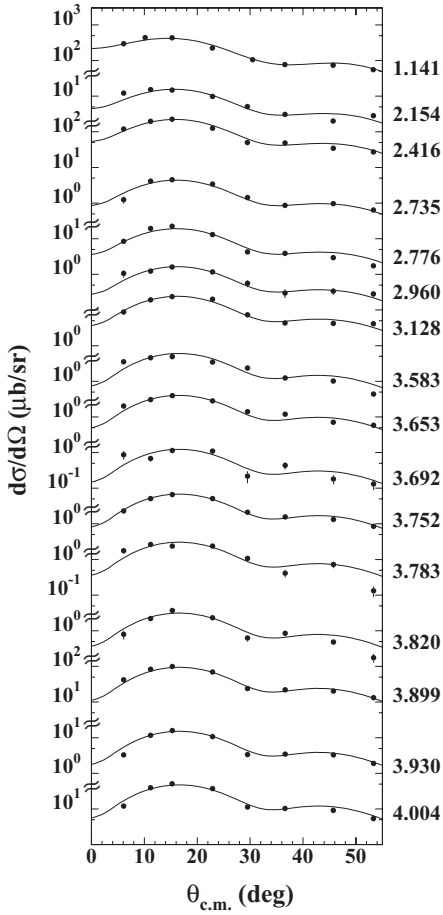


FIG. 9. Differential cross sections for the excitation of $2^+$ states by the $^{124}$Sn$(p,t)^{122}$Sn reaction. See fig. 2 for details.

*3.771 MeV.* The differential cross section of this level, not reported in NDS [6], is reasonably reproduced by an $L=4$ transfer. Present assignment of this new level is $J^\pi = 4^+$.

*3.805 MeV.* Two close levels are reported in NDS [6], the first at 3805.5 keV with $J^\pi = 4^+$ and the second at 3806.02 keV with $J^\pi = 2^+$. In our study we reproduce the angular distribution quite well by considering an unresolved doublet with $J^\pi = 4^+$ (60%) and $J^\pi = 2^+$ (40%).

*3.843 MeV.* In the adopted level scheme [6] a level is reported at 3843.66 keV with $J^\pi = 2^+$,3. In our measurement we reasonably reproduce the angular distribution of this weakly populated state with an $L=2$ transfer. Present assignment $J^\pi = 2^+$ removes the ambiguity of the NDS assignment.

### B. $^{124}$Sn$(p,t)^{122}$Sn reaction

Table II reports the spectroscopic information on $^{122}$Sn, deduced from the present experiment and compared with information available in the literature [7]. We have observed 63 transitions in $^{122}$Sn, up to an excitation energy of ∼4 MeV, of which with respect to the NDS compilation [7], 29 assignments have been confirmed, 13 ambiguities removed, 17 new levels have been observed and identified in $J^\pi$, and two new assignments have been carried out. Two unresolved doublets

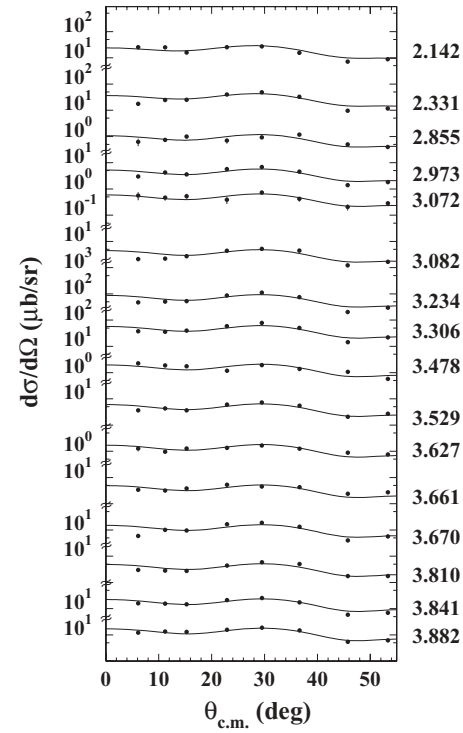


FIG. 10. Differential cross sections for the excitation of $4^+$ states by the $^{124}$Sn$(p,t)^{122}$Sn reaction. See Fig. 2 for details.

have been observed, giving two new assignments, and two ambiguities have been removed.

In this section we discuss the proposed assignments for the levels observed in the present measurement, new or corresponding to the reported ones in the NDS compilation [7] with uncertain $J^\pi$ or without $J^\pi$ assignment, together with the two unresolved doublets.

*2.654 MeV.* In the adopted level scheme [7] two close levels are reported, the first at 2653.00 keV with $J^\pi = 6^-$

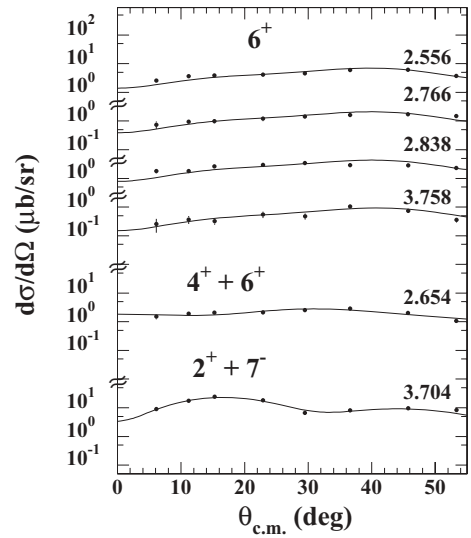


FIG. 11. Differential cross sections for the excitation of $6^+$ states and two doublets at 2.654 MeV, and 3.704 MeV by the $^{124}$Sn$(p,t)^{122}$Sn reaction. See Fig. 2 for details.

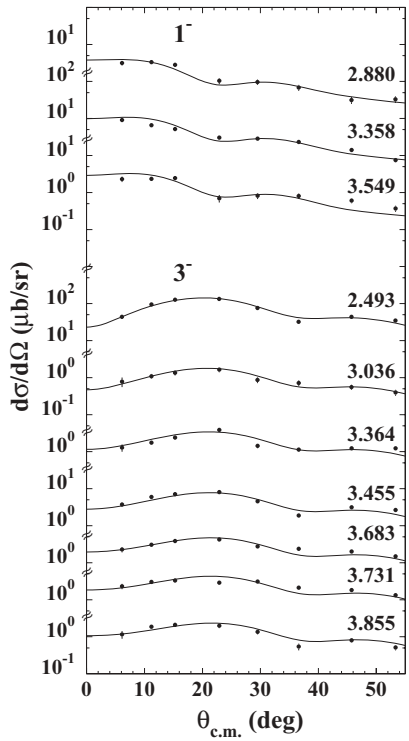


FIG. 12. Differential cross sections for the excitation of $1^-$ and $3^-$ states by the $^{124}$Sn$(p,t)^{122}$Sn reaction. See Fig. 2 for details.

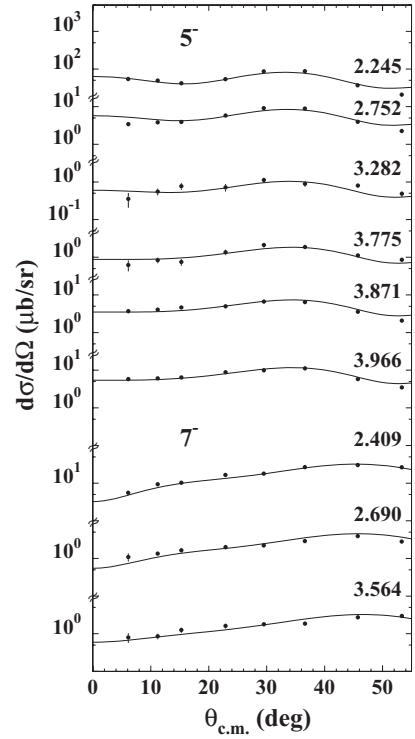


FIG. 13. Differential cross sections for the excitation of $5^-$, and $7^-$ states by the $^{124}$Sn$(p,t)^{122}$Sn reaction. See Fig. 2 for details.

deduced from a $\beta^-$ decay study of $^{122}$In (10.8 s) [28–30], $(n,n'\gamma)$ reaction [32,33], the second at 2657 keV, identified in $(p,t)$ reaction studies [5,37] without $J^\pi$ assignment. The measured angular distribution is rather featureless and is accurately reproduced by considering an unresolved doublet with assignment $J^\pi = 6^+$ (50%) and $J^\pi = 4^+$ (50%).

*2.690 MeV.* The NDS compilation [7] reports a level at 2690.04 keV with a tentative assignment $J^\pi = (8^+)$, inferred from a study of the energy dependence of the $^{124}$Sn$(p,t)^{122}$Sn reaction [37]. In our measurement the 2.690-MeV level angular distribution is quite well reproduced by an $L = 7$ transfer. Present assignment $J^\pi = 7^-$.

*2.766 MeV.* Reference [7] reports a level at 2765.6 keV with tentative assignment $J^\pi = (10^+)$, deduced from $(p,t)$ [37] and $(p,p')$ reaction [31] studies. In the present experiment an $L = 6$ transfer is consistent with the measured angular distribution. Present assignment $J^\pi = 6^+$.

*2.838 MeV, 2.855 MeV.* The NDS compilation [7] reports the levels at 2837.88 keV and 2855.47 keV with $J^\pi = 6^-$ and $J^\pi = 4^-$, respectively, deduced from $(n,n'\gamma)$ study [32,33]. The nature of the $\gamma$-ray decay for these levels is $M1 + E2$. Very close in energy to these levels we have identified two weakly populated transitions at 2.838 and 2.855 MeV. We reproduce the angular distributions with an $L = 6$ and $L = 4$ transfer, respectively. Present assignments $J^\pi = 6^+$ and $J^\pi = 4^+$, respectively.

*2.868 MeV.* A level at 2867.73 keV is reported in NDS [7] without spin and parity assignment. The shape of the angular distribution we measured is typical of an $L = 0$ transfer. Present assignment $J^\pi = 0^+$.

*2.880 MeV.* A level at 2879.79 keV with $J^\pi = 1^+, 2^+$ is reported in NDS [7], derived from a $^{122}$Sn$(n,n'\gamma)$ study [32]. In our measurement, the differential cross section for the level at 2.880 MeV is reproduced by an $L = 1$ transfer and the present assignment is $J^\pi = 1^-$.

*2.960 MeV.* In the adopted level scheme [7] a level is reported at 2959.12 keV, $J^\pi = 4^+$ from an $(n,n'\gamma)$ reaction study [32]. In our experiment the angular distribution is compatible with an $L = 2$ transfer. Presumably this level does not correspond to the level at 2959.12 keV. Present assignment $J^\pi = 2^+$.

*3.072 MeV.* At this energy no level is given in the adopted level scheme [7]. In our experiment the angular distribution of this weakly populated level is reasonably reproduced by an $L = 4$ transfer. Present assignment $J^\pi = 4^+$.

*3.206 MeV.* The NDS compilation [7] gives a positive parity level at 3206.25 keV with tentative $J = (0)^+$ assignment. The shape of measured angular distribution is distinctive of an $L = 0$ transfer. Present assignment $J^\pi = 0^+$ removes the uncertainty.

*3.282 MeV.* An $L = 5$ transfer well reproduces the measured angular distribution of the level at 3.282 MeV. The present assignment is $J^\pi = 5^-$. In the NDS compilation [7] a level, at 3281.43 keV, without spin and parity assignment, which decays exclusively to the first excited $2^+$ state, is reported. This level must therefore differ from the $J^\pi = 5^-$ level we observe at 3.282 MeV.

*3.455 MeV, 3.478 MeV.* Reference [7] reports two levels at 3454.82 and 3478.60 keV observed in $(n,n'\gamma)$ [32] study and tentatively identified in the $(p,p')$ reaction [16] as $L = (3)$

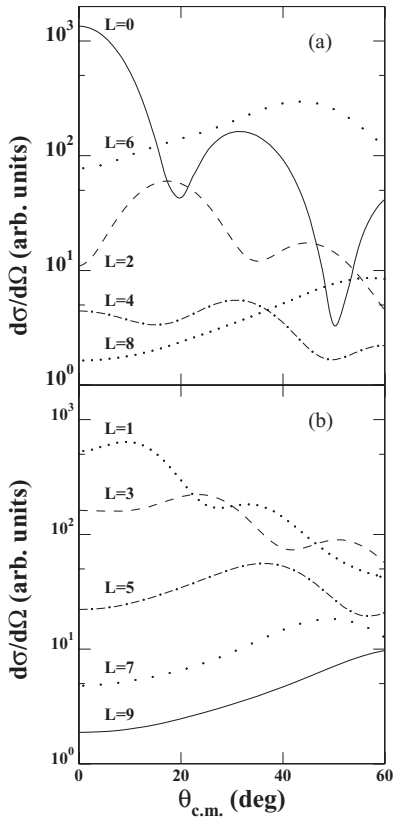


FIG. 14. Calculated differential cross sections for the $^{118}$Sn($p$,$t$)$^{116}$Sn reaction for transitions to a hypothetical level of $^{116}$Sn with an excitation energy of 3 MeV and given $L$ transfer: (a) even $L$ transfers, (b) odd $L$ transfers. The cluster DWBA calculations have been made using the set of optical model parameters of Table III.

and $L=(7)$ transfers, respectively. In our study the differential cross sections of the levels at 3.455 and 3.478 MeV are reasonably well reproduced by $L=3$ and $L=4$ transfer, respectively. Present assignments $J^\pi=3^-$ and $J^\pi=4^+$, respectively.

*3.529 MeV.* The NDS compilation [7] reports a level at 3530.71 keV with the tentative assignment $(7^-, 8^-)$, inferred from the study of the $\beta^-$ decay (10.8 s) of an $^{122}$In isomer [30]. In our experiment the 3.529-MeV level angular distribution is compatible with an $L=4$ transfer. Present assignment $J^\pi=4^+$.

*3.549 MeV.* In the adopted level scheme [7], a level at 3548.66 keV is listed with $J^\pi=2^+$, deduced from the study of $^{122}$In $\beta^-$ decay (1.5 s) [29] and from the ($n$,$n'\gamma$) reaction [32]. This level presents a 100% decay branch to the first excited $2^+$ state of $^{122}$Sn. Our measured angular distribution is consistent with an $L=1$ transfer and the present assignment is $J^\pi=1^-$. This level does not correspond to the level reported in the NDS compilation [7] at 3548.66 keV.

*3.564 MeV.* An $L=7$ transfer reproduces well the measured angular distribution of the level at 3.564 MeV, so the present assignment is $J^\pi=7^-$. The NDS compilation [7] reports a level without $J^\pi$ assignment at 3568.14 keV, which decays exclusively to the first excited $2^+$ state. This 3568.14-keV

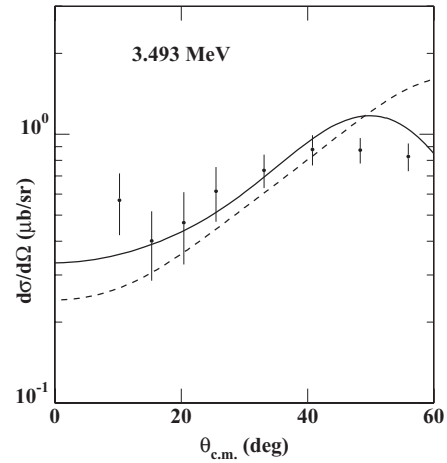


FIG. 15. Comparison of measured differential cross sections (dots) with calculations based on assumed $L$ transfers, relative to the 3.493-MeV level populated in the $^{118}$Sn($p$,$t$)$^{116}$Sn reaction. Solid line corresponds to $7^-$; dashed line to $8^+$.

level must therefore be different from the $J^\pi=7^-$ level that we observe at 3.564 MeV.

*3.653 MeV, 3.661 MeV, 3.683 MeV, 3.692 MeV.* At these energies no levels are given in the adopted level scheme [7]. We reproduce the angular distributions of these levels by considering $L=2$, $L=4$, $L=3$, and $L=2$ transfers, respectively. Present assignments for these levels are $J^\pi=2^+$, $J^\pi=4^+$, $J^\pi=3^-$, and $J^\pi=2^+$, respectively.

*3.704 MeV.* Two close levels are reported in the NDS compilation [7], the first at 3703.38 keV with tentative $J^\pi=(7^-, 8^-, 9^-)$ inferred from $^{122}$In $\beta^-$ decay (10.8 s) study [30], and the second at 3704.9 keV with tentative $J^\pi=(2^+)$ deduced from a ($n$,$n'\gamma$) reaction measurement [32]. In the present study we reproduce quite well the angular distribution of this transition by considering an unresolved

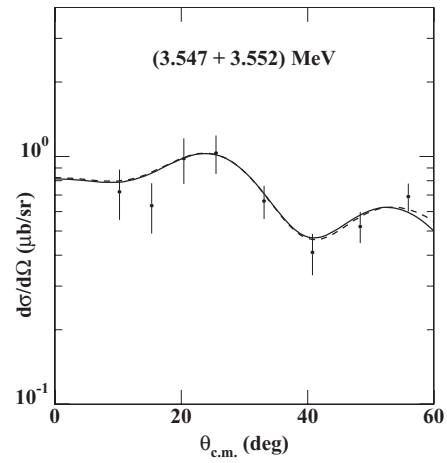


FIG. 16. Comparison of measured differential cross sections (dots) with calculations based on mixtures of assumed $L$ transfers, relative to the 3.549-MeV transition populated in the $^{118}$Sn($p$,$t$)$^{116}$Sn reaction. Solid line corresponds to 30% $8^+$, 70% $3^-$; dashed line to 30% $9^-$, 70% $3^-$.

doublet with $J^\pi = 7^-$ (30%) and $J^\pi = 2^+$ (70%). Present assignments remove the uncertainties.

*3.731 MeV.* In our analysis, the angular distribution of the tritons populating the 3.731-MeV level is compatible with an $L = 3$ transfer, and on this basis we assign it to have $J^\pi = 3^-$. The NDS compilation [7] reports a level at 3730.00 keV without spin and parity assignment, observed in the $(n,n'\gamma)$ [32] and $(p,p')$ reactions [16]. This 3730.00-keV level decays only to the first excited $2^+$ and second excited $4^+$ levels. It seems unlikely that a $3^-$ level would decay only to $2^+$ and $4^+$ levels, when there are several available odd-parity levels it could reach via $E2 + M1$ transitions. In fact the $E1$ transition rates are expected to be very small based on the values which have been measured for Sn isotopes around $^{122}$Sn [50]. This is consistent with the shell-model description, where the only contributions to the $E1$ transitions arise from core polarization. Therefore we conclude that the $J^\pi = 3^-$ level we populate in the $(p,t)$ reaction is not the same as the 3730.00-keV level.

*3.758 MeV.* In our study this transition is weakly populated, and a reasonable reproduction of the angular distribution is obtained assuming an $L = 6$ transfer, so the present assignment is $J^\pi = 6^+$. This level must therefore differ from the $J^\pi = 1$, $2^+$ level at 3758.51 keV observed in the $(n,n'\gamma)$ [32,33] and $(\gamma,\gamma')$ [12] reactions, as reported in the adopted level scheme [7].

*3.775 MeV.* In our measurement, the transition to the level at 3.775 MeV is consistent with $L = 5$ transfer, so the present assignment is $J^\pi = 5^-$. In the adopted level scheme [7] a level seen in the $(n,n'\gamma)$ [32] and $(p,p')$ reactions [16] is reported at 3777.0 keV without spin and parity assignment. It decays exclusively to the first excited $2^+$ state, and is therefore not the $J^\pi = 5^-$ level at 3.775 MeV that we populate in the $(p,t)$ reaction.

*3.783 MeV, 3.810 MeV.* In the adopted level scheme [7] two levels are reported: the first at 3782.84 keV with tentative assignment $J^\pi = (4^+)$, deduced from a study of $^{122}$In $\beta^-$ decay (10.3 s) [30] and $(n,n'\gamma)$ [30]; the second at 3810 keV with positive parity deduced from $L = 4$ transfer, observed in the $(t,\alpha)$ reaction [39]. In our measurement the transitions to 3.783 and 3.810 MeV are consistent with $L = 2$ and 4 transfer, respectively. Present assignments $J^\pi = 2^+$ and $J^\pi = 4^+$, respectively. The present assignments remove the uncertainty in NDS compilation.

*3.841 MeV.* In the adopted level compilation [7], a level is reported at 3840.65 keV with tentative $J^\pi = (4^+)$, deduced from a study of the decay scheme for the 10.5 s $^{122}$In isomer [30]. In our measurement, we reproduce the angular distribution quite well, assuming an $L = 4$ transfer and we assign $J^\pi = 4^+$ to this level, removing the uncertainty.

*3.855 MeV.* At this energy no level is given in the adopted level scheme [7]. The level we observe is weakly populated and is accurately reproduced by an $L = 3$ transfer. We assign $J^\pi = 3^-$ to this level.

*3.871 MeV.* The angular distribution of the level we observe at 3.871 MeV is reproduced well with $L = 5$ transfer. On this basis we assign it to have $J^\pi = 5^-$. This level must therefore differ from the $J^\pi = 1$, $2^+$ level at 3871.1 keV, which decays exclusively to the ground state $0^+$. The 3871.1-keV level is inferred from nuclear resonance fluorescence measurements [12], as reported in the adopted level scheme [7].

*3.899 MeV.* In the adopted level scheme [7], two levels are given: the first at 3899.68 keV with $J^\pi = 0^+$, $1^+$, $2^+$ populated in the decay of $^{122}$In (1.5 s) [29] and (10.3 s) [30]; the second at 3900 keV without spin and parity assignment, populated in the $(p,p')$ reaction [16]. The DWBA analysis of the angular distribution in Ref. [16] suggests a tentative $L = (2{+}4)$ transfer. In our measurement the level at 3.899 MeV is strongly populated and the angular distribution is very well reproduced by an $L = 2$ transfer. Present assignment $J^\pi = 2^+$.

*3.930 MeV.* In Ref. [7], a level is given at an energy of 3929.9 keV with $J^\pi = 1, 2^+$ deduced from the $(n,n'\gamma)$ reaction [32]. In our case the angular distribution of the tritons feeding the 3.930-MeV level is well reproduced by an $L = 2$ transfer. We assign $J^\pi = 2^+$, removing the ambiguity.

*3.966 MeV.* In the adopted level scheme [7], a level is listed at (3974±7) keV without spin and parity assignment, observed in $(p,p')$ [16] and $(t,\alpha)$ [39] reactions. In our measurement, an $L = 5$ transfer accurately reproduces the shape of the angular distribution. Present assignment is $J^\pi = 5^-$.

*4.004 MeV.* In Ref. [7] a level is given at 4004.0 keV with a tentative $J^\pi = (2^+)$ assignment, derived from $\gamma(\theta)$ and linear polarization data in an $(n,n'\gamma)$ reaction study [32]. We accurately reproduce the angular distribution of the strongly populated level at 4.004 MeV with an $L = 2$ transfer. Present assignment $J^\pi = 2^+$ removes the uncertainty.

## V. SHELL-MODEL CALCULATIONS

Consistent with our previous investigations of $^{110,114,118,120}$Sn [1–4], in the present shell-model study of $^{122}$Sn and $^{116}$Sn we employ a realistic two-body effective interaction. We start by assuming $^{132}$Sn as a closed core, with the 10 and 16 valence neutron holes occupying the five levels $0g_{7/2}$, $1d_{5/2}$, $1d_{3/2}$, $2s_{1/2}$, and $0h_{11/2}$ of the 50-82 shell. The matrix elements of the neutron-neutron effective interaction $V_{\rm eff}$ in the hole-hole representation are the same as those used in our previous paper on $^{118}$Sn [3]. For the sake of completeness, however, we give here a sketch of our procedure for deriving $V_{\rm eff}$.

We start from the CD-Bonn nucleon-nucleon ($NN$) potential [51] and renormalize its short-range repulsion by means of the $V_{\rm low-k}$ approach [52]. The low-momentum potential obtained is then used to derive $V_{\rm eff}$ within the framework of the $\hat{Q}$-box folded diagram expansion [53], including diagrams up to second order in $V_{\rm low-k}$. The computation of these diagrams is performed within the harmonic-oscillator basis, inserting intermediate states composed of hole and particle states restricted to two major shells below and above the $Z = 50$ and $N = 82$ Fermi surfaces. The oscillator parameter is $\hbar\omega = 7.88$ MeV.

As regards the five single-hole (SH) energies, we adopt two different sets. For $^{122}$Sn they are (in MeV) $\epsilon^{-1}_{g_{7/2}} = 2.4$, $\epsilon^{-1}_{d_{5/2}} = 1.6$, $\epsilon^{-1}_{s_{1/2}} = 0.3$, $\epsilon^{-1}_{d_{3/2}} = 0.0$, and $\epsilon^{-1}_{h_{11/2}} = 0.05$, while for $^{116}$Sn they are $\epsilon^{-1}_{g_{7/2}} = 3.0$, $\epsilon^{-1}_{d_{5/2}} = 2.6$, $\epsilon^{-1}_{s_{1/2}} = 0.85$, $\epsilon^{-1}_{d_{3/2}} = 1.2$, and $\epsilon^{-1}_{h_{11/2}} = 0.0$. These values have been determined, starting

TABLE IV. Comparison of calculated energies for $^{116}$Sn with those obtained from the present experiment. See text for details.

| $J^\pi$ | $E_{expt}$ (MeV) | $E_{calc}$ (MeV) | $J^\pi$ | $E_{expt}$ (MeV) | $E_{calc}$ (MeV) |
|---|---|---|---|---|---|
| $0^+$ | 0.000 | 0.000 | $5^-$ | 2.366 | 2.433 |
| | 1.757 | 1.902 | | 3.105 | 2.802 |
| | 2.027 | 2.206 | | 3.344 | 3.112 |
| | 2.546 | 2.631 | | 3.453 | 3.294 |
| | 3.194 | 3.358 | | | |
| | 3.724 | 3.711 | $7^-$ | 2.907 | 2.411 |
| | 3.836 | 3.811 | | 3.210 | 3.089 |
| | | | | 3.493 | 3.366 |
| $2^+$ | 1.294 | 1.453 | | 3.679 | 3.840 |
| | 2.112 | 2.011 | | 3.712 | 3.924 |
| | 2.225 | 2.199 | | | |
| | 2.650 | 2.681 | $9^-$ | 3.522 | 3.246 |
| | 2.843 | 2.928 | | | |
| | 2.960 | 3.057 | | | |
| | 3.088 | 3.135 | | | |
| | 3.227 | 3.241 | | | |
| | 3.231 | 3.323 | | | |
| | 3.416 | 3.456 | | | |
| | 3.469 | 3.651 | | | |
| | 3.586 | 3.684 | | | |
| | 3.805 | 3.732 | | | |
| $4^+$ | 2.391 | 2.323 | | | |
| | 2.530 | 2.723 | | | |
| | 2.790 | 2.845 | | | |
| | 2.801 | 3.012 | | | |
| | 3.046 | 3.083 | | | |
| | 3.096 | 3.486 | | | |
| | 3.157 | 3.533 | | | |
| | 3.278 | 3.695 | | | |
| | 3.506 | 3.795 | | | |
| $6^+$ | 3.251 | 3.229 | | | |
| | 3.648 | 3.484 | | | |
| | 3.739 | 3.731 | | | |

TABLE V. Comparison of calculated energies for $^{122}$Sn with those obtained from the present experiment. See text for details.

| $J^\pi$ | $E_{expt}$ (MeV) | $E_{calc}$ (MeV) | $J^\pi$ | $E_{expt}$ (MeV) | $E_{calc}$ (MeV) |
|---|---|---|---|---|---|
| $0^+$ | 0.000 | 0.000 | $1^-$ | 2.880 | 3.755 |
| | 2.088 | 1.970 | | 3.358 | 3.891 |
| | 2.530 | 2.385 | | 3.549 | 3.922 |
| | 2.676 | 2.976 | | | |
| | 2.868 | 3.305 | $3^-$ | 2.493 | 2.729 |
| | 3.206 | 3.465 | | 3.036 | 3.175 |
| | | | | 3.364 | 3.409 |
| $2^+$ | 1.141 | 1.378 | | 3.455 | 3.515 |
| | 2.154 | 2.361 | | 3.683 | 3.730 |
| | 2.416 | 2.481 | | 3.731 | 3.761 |
| | 2.735 | 2.545 | | 3.855 | 3.826 |
| | 2.776 | 3.016 | | | |
| | 2.960 | 3.155 | $5^-$ | 2.245 | 2.134 |
| | 3.128 | 3.344 | | 2.752 | 2.450 |
| | 3.583 | 3.379 | | 3.282 | 3.145 |
| | 3.653 | 3.488 | | 3.775 | 3.193 |
| | 3.692 | 3.546 | | 3.871 | 3.251 |
| | 3.704 | 3.595 | | 3.966 | 3.314 |
| | 3.752 | 3.750 | | | |
| | 3.783 | 3.793 | $7^-$ | 2.409 | 2.229 |
| | 3.820 | 3.826 | | 2.690 | 3.185 |
| | 3.899 | 3.897 | | 3.564 | 3.282 |
| | 3.930 | 3.972 | | 3.704 | 3.451 |
| $4^+$ | 2.142 | 2.077 | | | |
| | 2.331 | 2.614 | | | |
| | 2.654 | 3.014 | | | |
| | 2.855 | 3.243 | | | |
| | 2.973 | 3.275 | | | |
| | 3.072 | 3.451 | | | |
| | 3.082 | 3.585 | | | |
| | 3.234 | 3.642 | | | |
| | 3.306 | 3.681 | | | |
| | 3.478 | 3.822 | | | |
| | 3.529 | 3.849 | | | |
| | 3.627 | 3.877 | | | |
| | 3.661 | 3.904 | | | |
| | 3.670 | 3.938 | | | |
| | 3.810 | 3.982 | | | |
| | 3.841 | 4.020 | | | |
| | 3.882 | 4.086 | | | |
| $6^+$ | 2.556 | 2.284 | | | |
| | 2.654 | 3.030 | | | |
| | 2.766 | 3.417 | | | |
| | 2.838 | 3.592 | | | |
| | 3.758 | 3.607 | | | |

from the values taken from the experimental spectrum of $^{131}$Sn [54], through a fit to the yrast levels of $^{123}$Sn and $^{117}$Sn [50] having the same angular momentum and parity of the SH levels. However, it should be mentioned that although for $^{123}$Sn our calculated energies are in agreement with the experimental ones within tens of keV, for $^{117}$Sn we are not able to reproduce the experimental level ordering of the $1/2^+$ ground state and the first excited $3/2^+$ state. We find an inversion of these two states, with a spacing of 72 keV. As a matter of fact, this spacing is scarcely sensitive to the values of the SH energies.

The energies of both $^{116}$Sn and $^{122}$Sn have been obtained by carrying out full shell-model calculations using the Oslo shell-model code [55]. As in all our previous work on tin isotopes, we also compute the two-neutron spectroscopic amplitudes which are used to calculate the cross-section distributions for some states of $^{122}$Sn and $^{116}$Sn (see next section) within the framework of a microscopic DWBA approach. The spectroscopic amplitudes have been derived including in the model space states with seniority less than or equal to 4. More precisely, the wave functions of the $^{118}$Sn and the $^{124}$Sn ground states, as well as those of the $^{116}$Sn and $^{122}$Sn states, are obtained from calculations making use of the chain-calculation method described in Refs. [4,56], which is in fact based on the seniority scheme. We shall briefly comment on the accuracy of this approximation at the end of this section.

Let us start with $^{116}$Sn. We have calculated the spectrum of this nucleus up to an excitation energy of about 3.9 MeV and the energies obtained are compared with those measured in the present experiment in Table IV. It should be noted that we do not include in the comparison the observed $1^-$ and $3^-$ levels, as well as the $2^+$ level at 3.843 MeV and the four highest excited $4^+$ levels. As a matter of fact, in the considered energy interval the calculated level density for each of these angular

momenta is lower than the experimental one. In particular, no $1^-$ levels are predicted by our calculation and only two $3^-$ levels at 3.055 and 3.338 MeV are obtained, versus the seven observed $3^-$ levels. For all the other levels populated in the present experiment we have tried to establish a correspondence with the calculated ones as shown in Table IV.

We see that the agreement between theory and experiment for the positive-parity states is very good, the discrepancies in the excitation energies being less than 200 keV for all the levels except for the $4^+$ levels starting from the experimental level at 3.096 MeV. For these levels, the calculated energies overestimate the experimental ones by 350–400 keV. It is therefore plausible that the theoretical levels corresponding to the four highest observed levels with $J^\pi = 4^+$ lie above 3.9 MeV.

As regards the negative-parity levels, we see that, in contrast to the positive-parity levels, the energies of most of them are underestimated by the theory. For the yrast $7^-$ level, the calculated energy is 500 keV lower than the measured one, while the differences between theory and experiment for all the other levels range from 70 to 300 keV.

As a final point on $^{116}$Sn, we propose for the observed level with no firm spin-parity assignment, $(8^+, 9^-)$, at 3.549 MeV the association to the calculated yrast $8^+$ level at 3.34 MeV. The yrast $9^-$ level is in fact predicted by our calculation to be above 3.9 MeV.

We now compare the experimental and theoretical excitation energies of $^{122}$Sn, for which shell-model calculations have been performed up to 4-MeV excitation energy. This is done in Table V, where we have included all the levels observed in the present experiment, except the $2^+$ level at 4.004 MeV. In fact, for $J^\pi = 2^+$ we predict only 16 levels in the considered energy interval, namely one level less than the 17 observed levels. For each other value of $J^\pi$, it was possible to establish a tentative one-to-one correspondence between the observed levels and the lowest-lying calculated ones. We see that in most cases the observed energies are overestimated by the theory, aside from the $5^-$ and $7^-$ levels which are all predicted to lie below the observed ones. As regards the quantitative agreement, this is not as good as that found for $^{116}$Sn. In fact, the discrepancies between calculated and observed excitation energies range from few tens of keV to about 0.9 MeV for the first $1^-$ level. However, for only 17 out of the 63 compared levels does this discrepancy exceeds 300 keV.

As mentioned above, the eigenstates entering the two-particle spectroscopic amplitudes needed in the microscopic DWBA calculation have been obtained within the seniority-truncated shell model by means of the chain-calculation method [4,56] including states up to $v = 4$. Let us close this section with some comments which give an insight into the accuracy of this kind of calculation.

To this end, we focus on $^{116}$Sn for which our results could be more significantly affected by the adopted approximation scheme because of the larger number of neutron holes with respect to $^{122}$Sn. We have compared the full shell-model energies of $^{116}$Sn reported in Table IV with the seniority-truncated energies of the states involved in the calculation of the cross-section distributions. As it was to be expected, it turns out that all energies are overestimated by the approximate calculation. However, the differences between the results of the two calculations do not exceed 200 keV for most of the states. As a matter of fact, the $v > 4$ components seem to play a more significant role only for a few high-lying levels whose seniority-truncated energies are about 400 keV above the exact ones

As regards the ground-state energy both calculations give the same result. This state is in fact dominated by the $v = 0$ component with a percentage of 98%. To test its wave function we have considered the occupation numbers. It turns out that there is only a 1% increase in the occupation number of the $0g_{7/2}$ level when going from the exact to the approximate calculation. Concerning the occupation numbers of the other yrast states, we have found that the difference between the results of the two calculations reaches at most 10%.

## VI. MICROSCOPIC DWBA CALCULATIONS

In this section, we will use our calculated shell-model eigenstates to try to understand the measured differential cross sections for the $^{124}$Sn$(p,t)^{122}$Sn and $^{118}$Sn$(p,t)^{116}$Sn reactions. We assume these processes are *direct* reactions, which implies that the only degrees of freedom to be considered are those of the incident proton and the transferred neutrons. Starting with the target wave function, one must therefore project out the degrees of freedom of the target nucleons that are not involved in the transfer. What remains is the wave function of the transferred neutrons, in the form,

$$\sum_{n_1,\ell_1,j_1;n_2,\ell_2,j_2} S^J_{n_1,\ell_1,j_1;n_2,\ell_2,j_2} \times \frac{[\psi^{n_1,\ell_1,j_1}(\mathbf{r}_1,\sigma_1)\psi^{n_2,\ell_2,j_2}(\mathbf{r}_2,\sigma_2)]^J_M - [\psi^{n_1,\ell_1,j_1}(\mathbf{r}_2,\sigma_2)\psi^{n_2,\ell_2,j_2}(\mathbf{r}_1,\sigma_1)]^J_M}{2\left(1+\delta_{n_1,n_2}\delta_{\ell_1,\ell_2}\delta_{j_1,j_2}\right)}. \quad (1)$$

The $S^J_{n_1,\ell_1,j_1;n_2,\ell_2,j_2}$ coefficients entering here are the spectroscopic amplitudes, which are calculated from the target and residual shell-model eigenstates. The $\psi^{n_i,\ell_i,j_i}_{m_i}(\mathbf{r}_i,\sigma_i)$ are single-neutron shell-model orbitals. It is an important feature of this transfer mechanism that the different transferred configurations contribute coherently. Our treatment makes the further assumption that the only part of the target two-neutron wave function that contributes to the reaction is the part where the two neutrons have the same relative motion that they will have in the outgoing triton, namely with zero relative orbital angular momentum, and zero total intrinsic spin angular momentum. When this component is projected out of Eq. (1), the result is a function of the position of the two-neutron mass center, $F(R)Y^J_M(\hat{\mathbf{R}})$, which serves as the form

factor of a DWBA calculation. Details of these calculations are given elsewhere (see Ref. [1] and further references given there).

The DWBA calculations were done with the program TWOFNR [45], with the optical parameters listed in Table III, the same optical parameters that were used in the cluster transfer calculation of Sec. III.

The two-neutron transfer theory that we have used, in which the transferred neutrons have zero intrinsic spin and zero relative orbital angular momentum, will only connect a natural-parity target state (such as a $0^+$ ground state), to natural parity daughter states. Furthermore, the neutron orbitals included in our shell-model space do not allow us to pick up a neutron pair coupled to $1^-$. Therefore, we have calculations only for $0^+$, $2^+$, $4^+$, $6^+$, $3^-$, $5^-$, $7^-$, $9^-$ daughter levels.

This theory does not yield absolute differential cross sections because it uses a collective interaction between the proton and the transferred neutrons, rather than a realistic interaction between the proton and the individual neutrons. However, it should successfully account for the shapes of the angular distributions, and the relative differential cross sections for different final states of the residual nuclei. If so, we should be able to find a single normalization factor for our theory, which would suffice for the comparisons to all measured angular distributions.

### A. Ground-state transitions

The strongest $(p,t)$ transitions are those that connect ground states of even-neutron nuclei. This is because these ground states are characterized by highly correlated neutron pairs

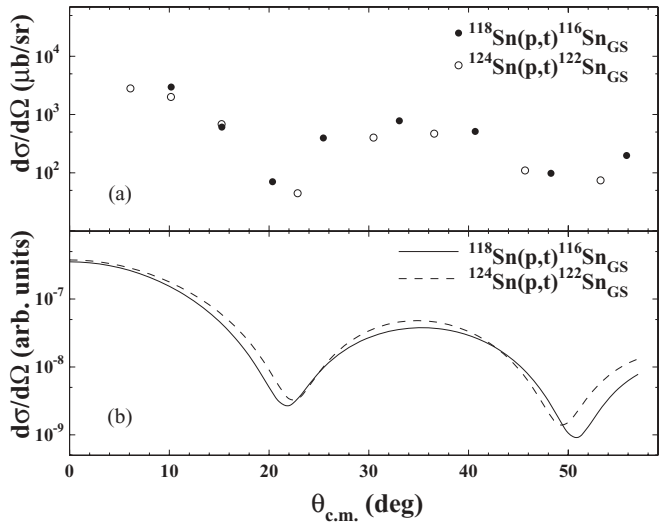


FIG. 17. (a) Measured differential cross sections for the population of the ground states by the $^{118}$Sn$(p,t)^{116}$Sn and $^{124}$Sn$(p,t)^{122}$Sn reactions. The error bars associated with the points are smaller than the symbols used to represent the points. (b) Microscopic calculations of the differential cross sections for the population of the ground states by the $^{118}$Sn$(p,t)^{116}$Sn and $^{124}$Sn$(p,t)^{122}$Sn reactions. The same arbitrary cross-section units are used for both reactions.

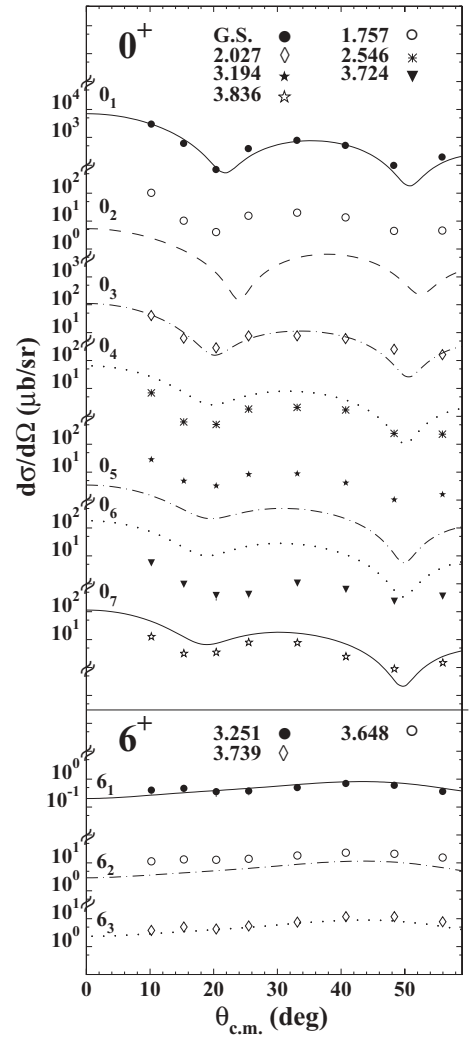


FIG. 18. Comparison between experimental and calculated cross sections for $0^+$ and $6^+$ final states of $^{116}$Sn. The lines represent results of the microscopic calculations of the differential cross sections (in $\mu$b/sr) as a function of center-of-mass angle (in degrees). The subscripts 1, 2, ... associated with the lines indicate the calculated energy ranking of the corresponding state, with 1 representing the lowest state of given $J^\pi$. The error bars associated with the points are smaller than the symbols used to represent the points.

with intrinsic spin zero. The triton is small in size, and its neutrons are mostly in a singlet intrinsic spin state. Thus a direct two-neutron transfer reaction is well suited to connect ground states, and we can expect the theory to be most reliable in describing these transitions. Therefore, we begin our test of the microscopic wave functions and transfer theory with a comparison of the differential cross sections of the $^{124}$Sn$(p,t)^{122}$Sn and $^{118}$Sn$(p,t)^{116}$Sn ground-state transitions.

Figure 17(a) shows that these transitions are comparable in strength, but that at forward angles, and in the vicinity of the peak at 35°, the $^{118}$Sn$(p,t)^{116}$Sn ground-state transition is slightly stronger. However, Fig. 17(b) shows that this is not the prediction of our microscopic calculation. The difference between measurement and theory can be expressed by saying that the theory underpredicts the strength of the $^{118}$Sn$(p,t)^{116}$Sn

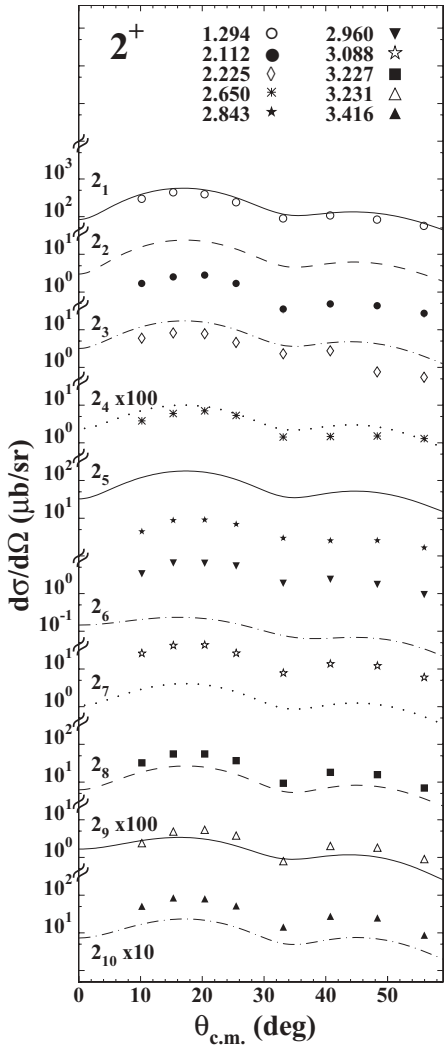


FIG. 19. Comparison between experimental and calculated cross sections for $2^+$ final states of $^{116}$Sn. Note that the data points correspond only to clearly resolved states. The doublets are not represented in the figure. See Fig. 18 for details.

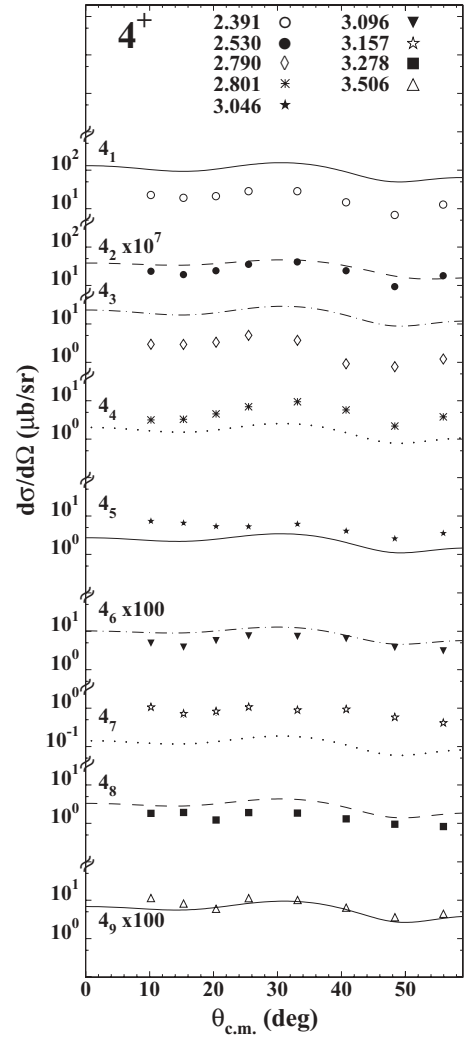


FIG. 20. Comparison between experimental and calculated cross sections for $4^+$ final states of $^{116}$Sn. Note that the data points correspond only to clearly resolved states. The doublets are not represented in the figure. See Fig. 18 for details.

ground-state transition by a factor of 0.55, relative to the strength of the $^{124}$Sn$(p,t)^{122}$Sn ground-state transition. There are two components to this prediction:

(i) The relative $^{118}$Sn$(p,t)^{116}$Sn and $^{124}$Sn$(p,t)^{122}$Sn spectroscopic amplitudes.
(ii) Dynamical effects, such as differences in $Q$ values, neutron separation energies, and nuclear sizes.

Comparison of the separate effects of these components shows that both indicate that the $^{124}$Sn$(p,t)^{122}$Sn ground-state transition should be the stronger one, in contrast to our measurements. This is an interesting result. It shows that somewhere between $^{118}$Sn$(p,t)^{116}$Sn and $^{124}$Sn$(p,t)^{122}$Sn, the physical situation changes in ways that our shell-model and reaction calculations do not represent. As a result of this discrepancy, we abandon our hope of accounting for all the $^{118}$Sn$(p,t)^{116}$Sn and $^{124}$Sn$(p,t)^{122}$Sn differential cross sections with a *single* overall normalization factor. Rather, we use different normalization factors for $^{118}$Sn$(p,t)^{116}$Sn and $^{124}$Sn$(p,t)^{122}$Sn, the $^{124}$Sn$(p,t)^{122}$Sn normalization factor being only 0.55 times as large as the $^{118}$Sn$(p,t)^{116}$Sn normalization factor.

### B. Discussion of individual levels

Figures 18–21 and 22–25 show comparisons between the calculated angular distributions and the observed data points for the $^{118}$Sn$(p,t)^{116}$Sn and $^{124}$Sn$(p,t)^{122}$Sn reactions, respectively. It is seen that, in every case, the theory gives a good account of the shape of the angular distribution, so that comparisons of magnitude can be done without specifying a particular angle.

The most remarkable general feature of the comparisons shown in Figs. 18–25 is the agreement between the predicted and observed magnitudes for the transitions to yrast states (the states of lowest energy for each angular momentum). This holds for all the yrast states in $^{122}$Sn, and for all except

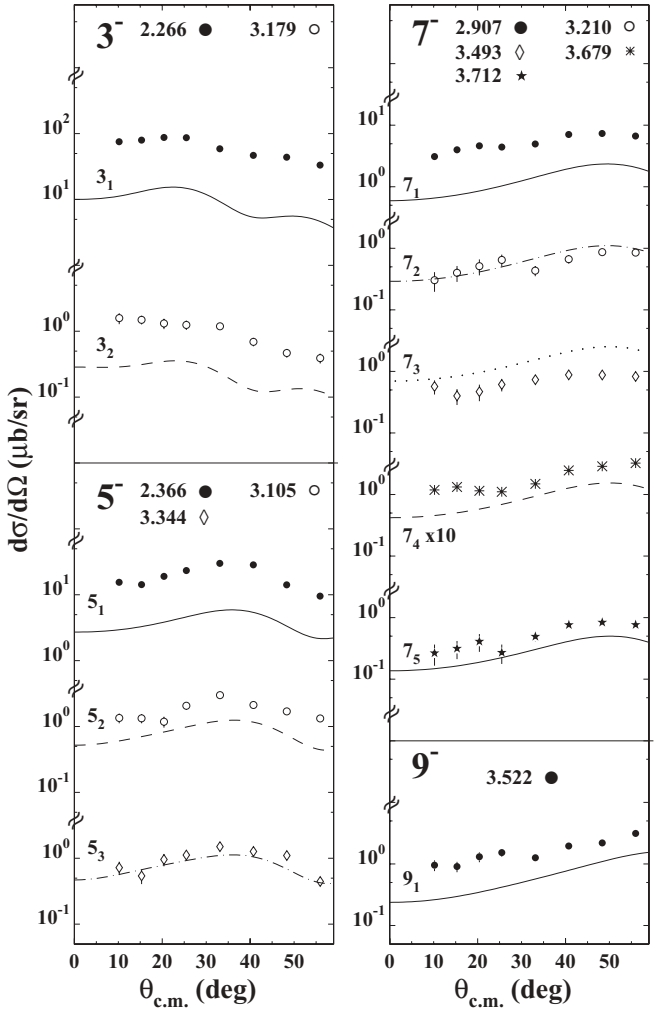


FIG. 21. Comparison between experimental and calculated cross sections for $3^-$, $5^-$, $7^-$ and $9^-$ final states of $^{116}$Sn. Note that the data points correspond only to clearly resolved states. The doublets are not represented in the figure. See Fig. 18 for details.

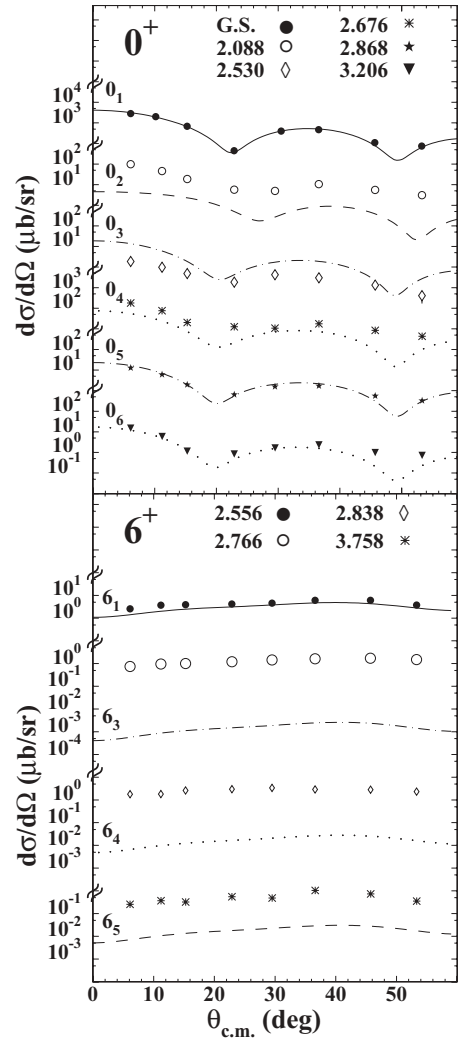


FIG. 22. Comparison between experimental and calculated cross sections for $0^+$ and $6^+$ final states of $^{122}$Sn. Note that the data points correspond only to clearly resolved states. The doublets are not represented in the figure. See Fig. 18 for details.

the $4_1^+$ level and the odd-parity levels of $^{116}$Sn. We conclude that our shell-model description of the structures of the states, together with our simplified microscopic description of the $(p,t)$ reaction, has the greatest validity for the yrast states. We can claim much less success for higher-energy states of each angular momentum. In some cases we predict approximately the correct magnitude; in others we significantly underpredict, or overpredict, the correct magnitude. Thus a detailed understanding of the populations of every state in the $(p,t)$ spectra to $^{116}$Sn and $^{122}$Sn will have to await more detailed descriptions of the structures of these states and/or the reaction mechanism.

### 1. $0^+$ transitions

The most striking feature of the $0^+$ spectra is the dominance of the ground-state transition. In $^{118}$Sn$(p,t)$, the ground-state transition is stronger than any other $0^+$ transition by a factor of about 39; in $^{124}$Sn$(p,t)$ the factor is about 27. The dominance of the ground-state transition is also a feature of the microscopic calculations, by factors of 27 in $^{118}$Sn$(p,t)$ and 68 in $^{124}$Sn$(p,t)$. This is a consequence of the dominant role of pairing in the structure of the microscopic calculations.

The most serious discrepancy between the data and our microscopic theory is in the population of the $0_2^+$ states. This is underpredicted in $^{118}$Sn$(p,t)$ by a factor of 40, and in $^{124}$Sn$(p,t)$ by a factor of 16. Evidently there are components in the $0_2^+$ states in the real $^{116}$Sn$(p,t)$ and $^{122}$Sn$(p,t)$ nuclei which are not present in our calculation, but which couple significantly to the target $^{118}$Sn and $^{124}$Sn states.

### 2. $2^+$ transitions

The population strength for the $2_1^+$ level, relative to the ground state $0_1^+$, is well described by the theory in both $^{118}$Sn$(p,t)$ and $^{124}$Sn$(p,t)$. However, in both reactions the population of the $2_2^+$ level is overpredicted by the theory by a factor of 8. It is clear from Figs. 19 and 23 that our calculation

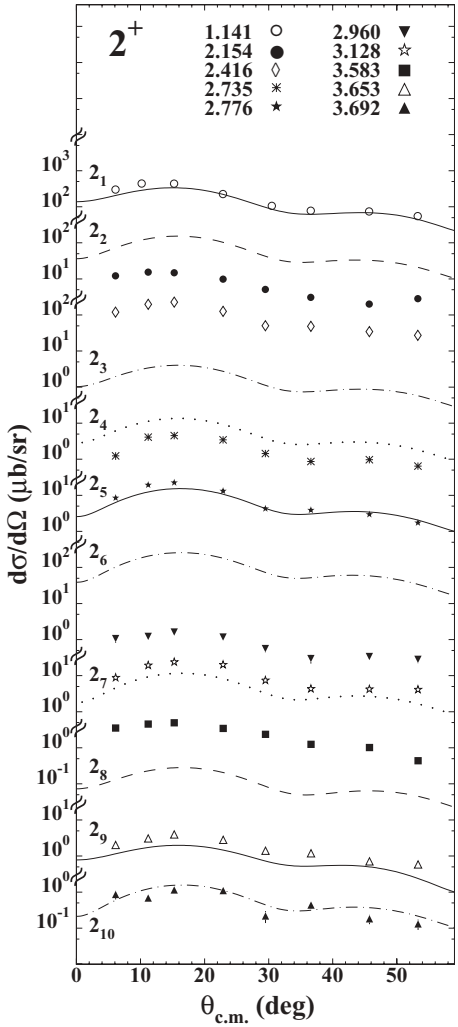


FIG. 23. Comparison between experimental and calculated cross sections for $2^+$ final states of $^{122}$Sn. Note that the data points correspond only to clearly resolved states. The doublets are not represented in the figure. See Fig. 18 for details.

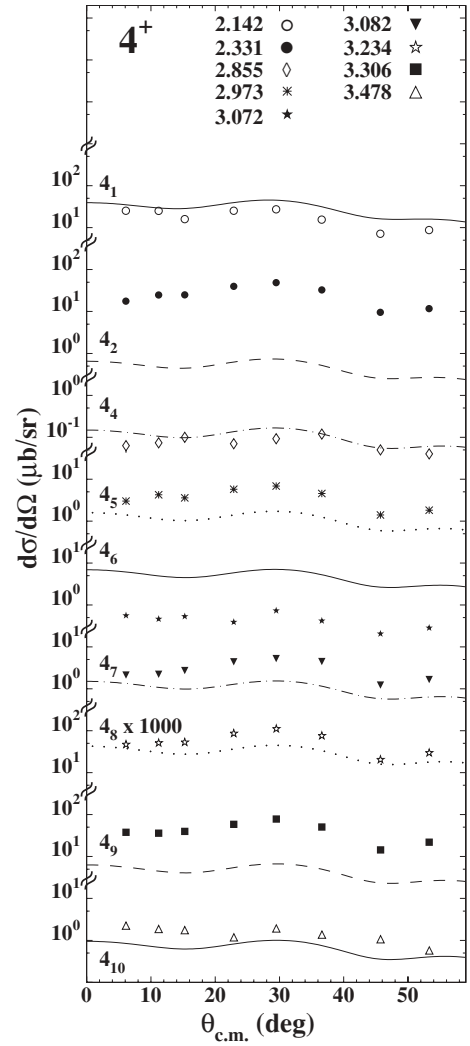


FIG. 24. Comparison between experimental and calculated cross sections for $4^+$ final states of $^{122}$Sn. Note that the data points correspond only to clearly resolved states. The doublets are not represented in the figure. See Fig. 18 for details.

is unable to give a detailed account of the populations of the higher excited $2^+$ levels. Some of the discrepancies are perhaps related to uncertainties of the calculated energies of the levels, which introduces ambiguities about which calculated angular distribution is to be compared to a particular observed angular distribution.

### 3. $4^+$ transitions

Figures 20 and 24 show that the calculated strength of $4_1^+$ agrees with experiment in the $^{124}$Sn$(p,t)^{122}$Sn case, but is about 5 times too large in the $^{118}$Sn$(p,t)^{116}$Sn case. The calculation predicts very strong population of $4_3^+$ in $^{122}$Sn, four times stronger than the population of $4_1^+$. This calculation is not shown in Fig. 24 because the $4_3^+$ level corresponds to the weakly populated $4^+$ level of the unresolved doublet at 2.654 MeV. On the other hand the experimental results show an excited $4^+$ level that is observed to have about four times the cross section of $4_1^+$, at an excitation energy of 3.234 MeV corresponding to the calculated $4_8^+$. The large predicted cross section is mainly from a strong $d_{5/2}d_{3/2}$ component in the transfer amplitude. This very strong excited $4^+$ level does not occur in $^{118}$Sn$(p,t)^{116}$Sn, either in theory or experiment.

### 4. $6^+$ transitions

The populations of the $6_1^+$ levels, in both $^{116}$Sn and $^{122}$Sn, are correctly given by the theory. The theory also gives a fairly good account of the populations of $6_2^+$ and $6_3^+$ levels in $^{116}$Sn, but the populations of the excited $6^+$ levels in $^{122}$Sn are strongly underpredicted.

### 5. $3^-$ transitions

The $3_1^-$ transition in $^{124}$Sn$(p,t)^{122}$Sn is correctly described by the microscopic theory. However, the $3_1^-$ transition in

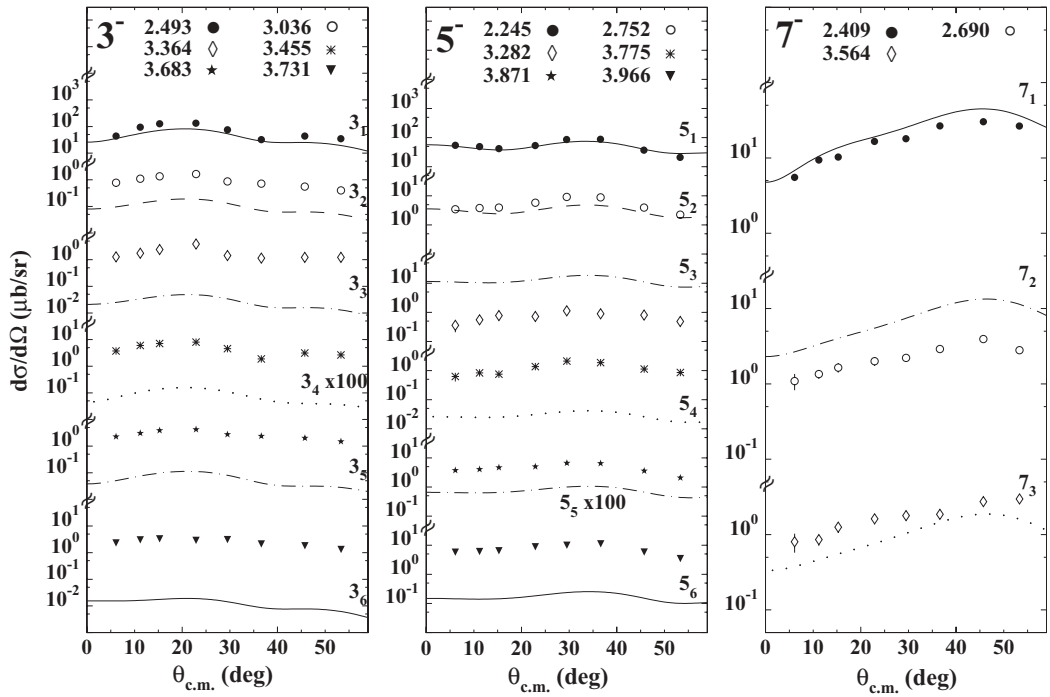


FIG. 25. Comparison between experimental and calculated cross sections for $3^-$, $5^-$, and $7^-$ final states of $^{122}$Sn. The lines represent results of the microscopic calculations of the differential cross sections (in $\mu$b/sr) as a function of center-of-mass angle (in degrees). The subscripts 1, 2,..., 6 associated with the lines indicate the calculated energy ranking of the corresponding state, with 1 representing the lowest state of given $J^\pi$. Error bars are shown for some $7^-$ states; in all other cases, the error bars are smaller than the symbols representing the measured differential cross sections. Note that the data points correspond only to clearly resolved states. The doublets are not represented in the figure.

$^{118}$Sn$(p,t)^{116}$Sn is underpredicted by a factor of 6. All the other $3^-$ transitions in both reactions are underpredicted.

#### 6. $5^-$ *transitions*

The situation here is similar to that of the $3^-$ transitions in $^{118}$Sn$(p,t)^{116}$Sn, with underpredictions of the cross sections for $5^-_1$ and $5^-_2$, while the $5^-_3$ level population is correctly given. Moreover, as for the $3^-$ transitions, the $5^-_1$ transition in $^{124}$Sn$(p,t)^{122}$Sn is well described. But here the $5^-_2$ transition is also well described.

#### 7. $7^-$ *transitions*

As is the case for the other odd-parity levels, $7^-_1$ is well accounted for in $^{124}$Sn$(p,t)^{122}$Sn, but is underpredicted in $^{118}$Sn$(p,t)^{116}$Sn.

#### 8. $9^-$ *transitions*

The $9^-_1$ transition in $^{118}$Sn$(p,t)^{116}$Sn is underpredicted by a factor of about 3.

## VII. SUMMARY

In high-resolution experiments, cross-section angular distributions in $(p,t)$ reactions induced on $^{118}$Sn$(p,t)^{116}$Sn at 24.6 MeV and on $^{124}$Sn$(p,t)^{122}$Sn at 25 MeV proton incident energies have been measured for 55 transitions to levels of $^{116}$Sn and 63 transitions to levels of $^{122}$Sn up to $\sim$3.850 MeV and $\sim$4.000 MeV of excitation energy, respectively.

We have assigned $J$ values and suggested parities to all the observed levels in both reactions by carrying out a DWBA analysis performed in finite range approximation, assuming a semimicroscopic dineutron cluster pickup mechanism.

Thirteen levels of $^{116}$Sn and 17 levels of $^{122}$Sn have been observed for the first time and identified in $J^\pi$. With respect to the $^{116}$Sn adopted levels, 32 previous assignments have been confirmed, and seven ambiguities have been removed. The three unresolved doublets give two confirmations, two new assignments, one tentative assignment, and one removed ambiguity. With respect to the $^{122}$Sn adopted levels, 29 previous assignments have been confirmed, 17 new levels have been identified in $J^\pi$, 13 ambiguities have been removed, and two new assignments have been carried out. The two unresolved doublets give two new assignments and two removed ambiguities.

A full shell-model study of the spectra of both $^{116}$Sn and $^{122}$Sn was performed using a two-body effective interaction derived from the CD-Bonn nucleon-nucleon potential. We have found that the agreement between theoretical and experimental excitation energies may be considered very satisfactory on the whole. For these two nuclei, having many valence holes, significant effects beyond the simple shell model could be expected. However, our results show that the degrees of freedom taken into account by our realistic shell-model calculation

play a crucial role in the description of their structure. In this context, it should emphasized that our effective interaction does not contain any adjustable parameters and, having been derived for the two-hole system, was not modified when dealing with 10 or 16 neutron holes. However, as discussed in Sec. V, the discrepancy between theory and experiment is rather large for some states. As regards the structure of the wave functions, which represents a further important test of the shell-model description, significant information comes out from the DWBA analysis of the present experiment, as is summarized in the following.

The microscopic calculations of differential cross sections are able to account for the ratios of the cross sections to yrast levels, in accord with the general expectation that these levels should have the simplest structure. The situation is less clear for other excited levels. In particular, the $0_2^+$ states are strongly underpredicted by our calculations, indicating that these states contain important components not included in our shell-model space. We are also unsuccessful in accounting for the observed ratio of the intensities of the transitions to the $^{116}$Sn and $^{122}$Sn ground states. This implies that it may be an oversimplification to regard these nuclei as essentially identical in structure, apart from the number of occupied neutron orbitals. These comparisons emphasize the usefulness of the $(p,t)$ reaction in providing stringent tests of microscopic descriptions of nuclear states.


[1] P. Guazzoni, L. Zetta, A. Covello, A. Gargano, B. F. Bayman, G. Graw, R. Hertenberger, H.-F. Wirth, and M. Jaskóla, Phys. Rev. C **74**, 054605 (2006).

[2] P. Guazzoni, L. Zetta, A. Covello, A. Gargano, G. Graw, R. Hertenberger, H.-F. Wirth, and M. Jaskóla, Phys. Rev. C **69**, 024619 (2004).

[3] P. Guazzoni, L. Zetta, A. Covello, A. Gargano, B. F. Bayman, T. Faestermann, G. Graw, R. Hertenberger, H.-F. Wirth, and M. Jaskóla, Phys. Rev. C **78**, 064608 (2008).

[4] P. Guazzoni, *et al.*, Phys. Rev. C **60**, 054603 (1999).

[5] D. G. Fleming, M. Blann, H. W. Fulbright, and J. A. Robbins, Nucl. Phys. A **157**, 1 (1970).

[6] J. Blachot, Nucl. Data Sheets **92**, 455 (2001).

[7] T. Tamura, Nucl. Data Sheets **108**, 455 (2007).

[8] K. Okano and Y. Kawase, Nucl. Instrum. Methods **108**, 503 (1973).

[9] Z. Gácsi and S. Raman, Phys. Rev. C **49**, 2792 (1994).

[10] S. Raman, T. A. Walkiewicz, S. Kahane, E. T. Jurney, J. Sa, Z. Gácsi, J. L. Weil, K. Allaart, G. Bonsignori, and J. F. Shriner Jr., Phys. Rev. C **43**, 521 (1991).

[11] L. I. Govor, A. M. Demidov, and I. V. Mikhailov, Yad. Fiz. **53**, 3 (1991) [Sov. J. Nucl. Phys. **53**, 1 (1991)]

[12] J. Bryssinck *et al.*, Phys. Rev. C **61**, 024309 (2000).

[13] A. Van Poelgeest, J. Bron, W. H. A. Hesselink, K. Allaart, J. J. A. Zalmstra, M. J. Uitzinger, and H. Verheul, Nucl. Phys. A **346**, 70 (1980).

[14] J. Bron, W. H. A. Hesselink, A. Van Poelgeest, J. J. A. Zalmstra, M. J. Uitzinger, H. Verheul, K. Heyde, M. Waroquier, H. Vincx, and P. Van Isacker, Nucl. Phys. A **318**, 335 (1979).

[15] A. Savelius *et al.*, Nucl. Phys. A **637**, 491 (1998).

[16] O. Beer, A. El Behay, P. Lopato, Y. Terrien, G. Vallois, and K. K. Seth, Nucl. Phys. A **147**, 326 (1970).

[17] H. Wienke, H. P. Blok, and J. Blok, Nucl. Phys. A **405**, 237 (1983).

[18] Y. S. Kim and B. L. Cohen, Phys. Rev. **142**, 788 (1966).

[19] S. Y. Van der Werf *et al.*, Phys. Lett. B **166**, 372 (1986).

[20] A. Bäcklin, N. G. Jonsson, R. Julin, J. Kantele, M. Luontama, A. Passoja, and T. Poikolainen, Nucl. Phys. A **351**, 490 (1981).

[21] N.-G. Jonsson, A. Bäcklin, J. Kantele, R. Julin, M. Luontama, and A. Passoja, Nucl. Phys. A **371**, 333 (1981).

[22] E. J. Schneid, A. Prakash, and B. L. Cohen, Phys. Rev. **156**, 1316 (1967).

[23] H. W. Fielding, R. E. Anderson, C. D. Zafiratos, D. A. Lind, F. E. Cecil, H. H. Wieman, and W. P. Alford, Nucl. Phys. A **281**, 389 (1977).

[24] D. G. Fleming, Can. J. Phys. **60**, 428 (1982).

[25] J. M. Schippers, J. M. Schreuder, S. Y. van der Werf, K. Allaart, N. Blasi, and M. Waroquier, Nucl. Phys. A **510**, 70 (1990).

[26] J. M. Schippers, Ph.D. thesis, Rijksuniversiteit Groningen, 1988.

[27] K. Yagi, Y. Saji, T. Ishimatsu, Y. Ishizaki, M. Matoba, Y. Nakajima, and C. Y. Huang, Nucl. Phys. A **111**, 129 (1968).

[28] H. C. Cheung, H. Huang, and J. K. P. Lee, Can. J. Phys. **57**, 460 (1979).

[29] B. Fogelberg and P. Carle, Nucl. Phys. A **323**, 205 (1979).

[30] S. Raman, T. A. Walkiewicz, L. G. Multhauf, K. G. Tirsell, G. Bonsignori, and K. Allaart, Phys. Rev. C **37**, 1203 (1988).

[31] I. Kumabe *et al.*, J. Phys. Soc. Jpn. **47**, 673 (1979).

[32] A. M. Demidov and I. V. Mikhailov, Izv. Akad. Nauk. SSSR, Ser. Fiz. **55**, 2112 (1991).

[33] L. I. Govor, A. M. Demidov, O. K. Zhuravlev, I. V. Mikhailov, and E. Yu Shkuratova, Yad. Fiz. **54**, 330 (1991) [Sov. J. Nucl. Phys. **54**, 196 (1991)].

[34] J. Bryssinck *et al.*, Phys. Rev. C **59**, 1930 (1999).

[35] R. Broda *et al.*, Phys. Rev. Lett. **68**, 1671 (1992).

[36] K. Yagi, Y. Aoki, C. Rangacharyulu, M. Matoba, M. Hyakutake, and J. Niidome, Phys. Lett. B **44**, 447 (1973).

[37] M. Matoba, K. Tsuji, K. Marubayashi, T. Shintake, K. Ohba, and T. Nomiyama, Phys. Rev. C **27**, 2598 (1983).

[38] J. Jänecke, F. D. Becchetti, and C. E. Thorn, Nucl. Phys. A **325**, 337 (1979).

[39] Z. Basrak, N. Cindro, and M. Turk, Nucl. Phys. A **299**, 381 (1978).

[40] H.-F. Wirth, H. Angerer, T. von Egidy, Y. Eisermann, G. Graw, and R. Hertenberger, in *Jahresbericth 2000, Beschleunigerlaboratorium München* (2001), p. 71.

[41] E. Zanotti, M. Bisenberger, R. Hertenberger, H. Kader, and G. Graw, Nucl. Instrum. Methods Phys. Res., Sect. A **310**, 706 (1991).

[42] J. R. Comfort, ANL Phys. Division, Informal Report PHYS-1970B, 1970 (unpublished).

[43] M. A. Nagarajan, M. R. Strayer, and M. F. Werby, Phys. Lett. B **68**, 421 (1977).

[44] M. Igarashi and K. I. Kubo, Phys. Rev. C **25**, 2144 (1982).

[45] M. Igarashi, computer code TWOFNR, 1977 (unpublished).

[46] F. G. Perey, Phys. Rev. **131**, 745 (1963).
[47] P. Guazzoni, L. Zetta, V. Yu. Ponomarev, G. Graw, R. Hertenberger, T. Faestermann, H.-F. Wirth, and M. Jaskóla, J. Phys. G: Nucl. Part. Phys. G **34**, 2665 (2007).
[48] P. Guazzoni, M. Jaskóla, V. Yu. Ponomarev, L. Zetta, G. Graw, R. Hertenberger, and G. Staudt, Phys. Rev. C **62**, 054312 (2000).
[49] J. M. Schippers, W. T. A. Borghols, M. A. Hofstee, R. F. Noorman, J. M. Schreuder, S. Y. van der Werf, and N. Blasi, Nucl. Phys. A **548**, 271 (1992).
[50] Data extracted using the NNDC Online Data Service from the ENSDF database (file revised as of January 21, 2011).
[51] R. Machleidt, Phys. Rev. C **63**, 024001 (2001).
[52] S. Bogner, T. T. S. Kuo, L. Coraggio, A. Covello, and N. Itaco, Phys. Rev. C **65**, 051301(R) (2002).
[53] L. Coraggio, A. Covello, A. Gargano, T. T. S. Kuo, and N. Itaco, Prog. Part. Nucl. Phys. **62**, 135 (2009), and references therein.
[54] B. Fogelberg *et al.*, Phys. Rev. C **70**, 034312 (2004).
[55] T. Engeland, the Oslo shell-model code, 1991–2006 (unpublished).
[56] A. Covello, F. Andreozzi, L. Coraggio, A. Gargano, and A. Porrino, in *Contemporary Nuclear Shell Model*, Lecture Series in Physics Vol. 482 (Springer-Verlag, Berlin, 1997).